

Intrinsic Topological Entanglement Entropy and the Strong Subadditivity

Chih-Yu Lo^{1,*} and Po-Yao Chang^{1,†}

¹*Department of Physics, National Tsing Hua University, Hsinchu 30013, Taiwan*

(Dated: November 11, 2024)

In $(2+1)d$ topological quantum field theory, topological entanglement entropy (TEE) can be computed using the replica and surgery methods. We classify all bipartitions on a torus and propose a general method for calculating their corresponding TEEs. For each bipartition, the TEEs for different ground states are bounded by a topological quantity, termed the intrinsic TEE, which depends solely on the number of entanglement interfaces $\pi_{\partial A}$, $S_{\text{iTEE}}(A) = -\pi_{\partial A} \ln \mathcal{D}$ with \mathcal{D} being the total quantum dimension. We derive a modified form of strong subadditivity (SSA) for the intrinsic TEE, with the modification depending on the genus g_X of the subregions X , $S_{\text{iTEE}}(A) + S_{\text{iTEE}}(B) - S_{\text{iTEE}}(A \cup B) - S_{\text{iTEE}}(A \cap B) \geq -2 \ln \mathcal{D} (g_A + g_B - g_{A \cup B} - g_{A \cap B})$. Additionally, we show that SSA for the full TEE holds when the intersection number between torus knots of the subregions is not equal to one. When the intersection number is one, the SSA condition is satisfied if and only if $\sum_a |\psi_a|^2 (\ln S_{0a} - \ln |\psi_a|) + |S\psi_a|^2 (\ln S_{0a} - \ln |S\psi_a|) \geq 2 \ln \mathcal{D}$, with S being the modular S -matrix and ψ_a being the probability amplitudes. This condition has been verified for unitary modular categories up to rank 11, while counterexamples have been found in non-pseudo-unitary modular categories, such as the Yang-Lee anyon.

Contents

I. Introduction	1	VI. Conclusion	19
A. Entanglement measures and the strong subadditivity	3	VII. Acknowledgments	20
B. Generalized surgery	3	A. Some related proof 1	20
II. Classification of bipartitions	4	B. Some related proof 2	20
A. Regularization of bipartitions	4	C. Edge approach	20
B. Classification of bipartitions	4	References	21
C. Canonical bipartitions on a torus	5		
III. The intrinsic TEE and TEE for general bipartitions	6	I. Introduction	
A. The intrinsic TEE and the topological RT formula	6	Topological orders [1] are phases of matter that are beyond the Ginzburg-Landau characterization [2]. A topologically ordered system is a gapped system that features robust ground state degeneracies and long ranged entanglement. Well-known examples include the fractional quantum Hall effect [3, 4], gapped quantum spin liquids [5] and $p_x + ip_y$ superconductors [6]. When such a system becomes infinitely gapped, its ground states can often be effectively described by a topological quantum field theory (TQFT).	
B. Vacuum state	7	A TQFT is a quantum field theory whose Lagrangian is topologically invariant. One famous example is the Chern-Simons theory where the topological invariant is associated with the knot invariant [7]. Axiomatically, TQFTs can be understood as functors from the category of $d+1$ dimensional manifolds to the category of Hilbert spaces associated with d dimensional quantum field theories [8]. These mappings are examples of the holographic principle in its simplest form, even predating its formalization [9, 10]. For instance, the Chern-Simons theory defined on a three-dimensional manifold is dual to the Wess-Zumino-Witten (WZW) theory on the two-dimensional boundary of the manifold. In this paper, we	
C. Generic state on R_2 bipartition	8		
D. Generic state on R_3 and R_m bipartition	11		
IV. The modified SSA of S_{iTEE}	13		
V. The SSA of S_{TEE}	14		
A. Isolating contractible regions	15		
1. $\Delta \mathcal{I}_{\text{iTEE}} \geq 0$	15		
2. $\Delta \mathcal{I}_{\text{gs}} < 0$ implies $\Delta \mathcal{I}_{\text{TEE}} \geq 0$	16		
B. Removing contractible isolated regions	16		
C. The SSA for S_{TEE} for ribbons	16		
1. $i_{AB} \geq 2$	17		
2. $i_{AB} = 0$	17		
3. $i_{AB} = 1$	18		
D. Violation of SSA for S_{iTEE}	19		

* chihyulo.jared@gmail.com

† pychang@phys.nthu.edu.tw

focus on $d = 3$ TQFTs, where the partition function of a three-dimensional manifold generates a quantum state on the Hilbert space of its two-dimensional boundary.

Topological entanglement entropy (TEE) is one of the key characteristics of topologically ordered systems [11, 12]. It is proposed that the entanglement entropy (EE) between a region A and its complement A^c can be expressed as

$$S_{EE}(A) = \alpha L_A + S_{TEE}(A), \quad (\text{I.1})$$

where α is a proportional constant, L_A is the length of ∂A and $S_{TEE}(A)$ is the TEE between A and A^c . TEE is a non-positive correction to the EE with the strong constraints in topologically ordered systems. This quantity has been numerically verified in various lattice models [13–19]. It can also be computed analytically through two main approaches: the bulk approach using the replica and surgery methods [20], and the edge approach using Ishibashi states [21–24]. Throughout this work, we mainly follow the bulk approach, which neglects the area contribution at the interfaces. Specifically, we derive the TEE for an arbitrary bipartition on a torus, showing that the TEE has a lower bound that depends only on the number of entangling interface components. This quantity, which we call the intrinsic TEE, is given by:

$$S_{iTEE}(A) := \min_{|\psi\rangle \in \mathcal{H}} S_{TEE}(A, |\psi\rangle), \quad (\text{I.2})$$

and is independent of the specific ground state. On a lattice, where ground state degeneracy may lead to uncertainty about the specific state, it is beneficial to focus on this ground-state-independent quantity. Furthermore, this minimally entangled state is preferred when applying the Density Matrix Renormalization Group (DMRG) method to compute the TEE [17].

In the context of holography, the leading contribution to the ground-state EE at the boundary is proportional to the area of the minimal surface anchored to the entanglement interface, as described by the Ryu-Takayanagi (RT) formula [25]. In TQFTs, where there is no unique ground state, it is natural to consider the minimally entangled ground state, which yields the intrinsic TEE of the interface. We will show that this intrinsic TEE depends purely on the number of boundary components of the interface. This leads to a topological version of the RT formula:

$$S_{iTEE}(A) = -\pi_{\partial A} \ln \mathcal{D}, \quad (\text{I.3})$$

where $\pi_{\partial A} = |\pi_0(\partial A)|$ is the number of interfaces between A, A^c , and $\mathcal{D} = \sqrt{\sum_a d_a^2}$ is the total quantum dimension which relates to the summing over all the superselection sectors (anyons) of the systems with each individual dimension d_a of a -type anyon. While the EE is proportional to the area of the minimal surface in the RT formula, the intrinsic TEE is proportional to the number of boundary components of that minimal surface.

A proof of the strong subadditivity (SSA) for entanglement entropy can be given geometrically using the RT formula [26], which leads to $S_{EE}(A) + S_{EE}(B) - S_{EE}(A \cup B) - S_{EE}(A \cap B) \geq 0$. Similarly, we apply Eq. (I.3) and topological arguments to show a modified version of the SSA for the intrinsic TEE

$$S_{iTEE}(A) + S_{iTEE}(B) - S_{iTEE}(A \cup B) - S_{iTEE}(A \cap B) \geq -2 \ln \mathcal{D}(g_A + g_B - g_{A \cup B} - g_{A \cap B}), \quad (\text{I.4})$$

where g_X is the genus of the surface X . Such modification term is bounded by

$$-1 \leq g_A + g_B - g_{A \cup B} - g_{A \cap B} \leq 1. \quad (\text{I.5})$$

We find that the standard SSA fails only when A and B consist of torus knot ribbons, and their intersection number is one.

On the other hand, the SSA for total TEE can be shown by the SSA for the EE together with Eq. (I.1) and the extensive property of the αL term. In this paper, we present a proof of SSA for TEE without relying on Eq. (I.1) up to a conjecture. First, we show that the conditional mutual information decreases only when contractible regions are isolated. Next, we prove that the conditional mutual information remains invariant under the removal of these isolated regions. By combining these two results, we can systematically remove all contractible subregions and reduce the problem to the case where regions A, B consist purely of torus knot ribbons. For these configurations, we classify the cases based on the intersection number i_{AB} between the torus knots of regions A and B . For $i_{AB} > 2$ and $i_{AB} = 0$, we are able to show that the SSA indeed holds. For $i_{AB} = 1$, we are able to show that the SSA is valid if and only if for all set of possible probability amplitudes $\{\psi_a\}_a$ subject to the constraint $\sum_a |\psi_a|^2 = 1$, the following inequality holds:

$$\sum_a |\psi_a|^2 (\ln d_a - \ln |\psi_a|) + |S\psi_a|^2 (\ln d_a - \ln |S\psi_a|) \geq 2 \ln \mathcal{D}, \quad (\text{I.6})$$

where S is the modular S -matrix and $d_a = S_{0a}$ are the quantum dimensions.

We have numerically verified that Eq. (I.6) holds for unitary modular tensor categories (UMTC) with rank less than 11 [27], including notable examples such as the Fibonacci anyons and the Semion model. We conjecture that Eq. (I.6) is valid for all UMTCs, and that it may impose implicit constraints on the modular data. On the other hand, for non-pseudo-unitary modular categories such as the Galois partner of Fibonacci anyon (Yang-Lee anyon), Eq. (I.6) can be violated. Nevertheless, the SSA for TEE can still be deduced using Eq. (I.1). This suggests that for non-pseudo-unitary modular categories, either the calculation of TEE or Eq. (I.1) itself requires modification.

The outline of this paper is as follows. In the remainder of this section, we briefly review the SSA condition

and generalize the surgery method. In Sec. II, we classify all possible bipartitions on a torus and discuss how to reduce them to canonical bipartitions. Readers familiar with these techniques may proceed directly to Sec. III. In Sec. III, we apply the replica method and generalized surgery to compute the TEE for canonical bipartitions, and explore the concept of intrinsic TEE. Sec. IV introduces the modified SSA for intrinsic TEE, supported by topological arguments. Finally, in Sec. V, we will present the proof for the SSA of the TEE up to Eq. (I.6), along with several low-rank examples illustrating both valid and invalid cases.

Let us begin by summarizing some key concepts that will be referenced throughout this paper.

A. Entanglement measures and the strong subadditivity

In the context of quantum information, given two disjoint subregions A, B , the mutual information between these regions is defined as

$$I(A : B) = S_{\text{EE}}(A) + S_{\text{EE}}(B) - S_{\text{EE}}(A \cup B), \quad (\text{I.7})$$

where

$$S_{\text{EE}}(A) = \text{Tr}(\rho_A \ln \rho_A) \quad (\text{I.8})$$

is the Von-Neumann entropy corresponding to the reduced density matrix $\rho_A = \text{Tr}_{A^c} \rho$. The mutual information quantifies the additional information that is not captured by A or B individually. Generally, A, B might not be the complement of each other.

When A and B intersect, the conditional mutual information further measures the additional information that remains unrepresented in the Venn diagram:

$$\begin{aligned} I(A : B | A \cap B) \\ = S_{\text{EE}}(A) + S_{\text{EE}}(B) - S_{\text{EE}}(A \cup B) - S_{\text{EE}}(A \cap B). \end{aligned} \quad (\text{I.9})$$

For simplicity, we denote the conditional mutual information as

$$\mathcal{I}_{\text{EE}}(A : B) := I(A : B | A \cap B). \quad (\text{I.10})$$

The strong subadditivity (SSA) of von Neumann entropy is expressed as:

$$S_{\text{EE}}(A \cup C) + S_{\text{EE}}(B \cup C) - S_{\text{EE}}(A \cup B \cup C) - S_{\text{EE}}(C) \geq 0. \quad (\text{I.11})$$

If we take $A' = A \cup C$ and $B' = B \cup C$, then the SSA can be rewritten as

$$S_{\text{EE}}(A') + S_{\text{EE}}(B') - S_{\text{EE}}(A' \cup B') - S_{\text{EE}}(A' \cap B') \geq 0, \quad (\text{I.12})$$

This is also equivalent to stating that the conditional mutual information is non-negative:

$$\mathcal{I}_{\text{EE}}(A' : B') \geq 0. \quad (\text{I.13})$$

Furthermore, the conditional mutual information is invariant under taking the simultaneous complement of both A and B ,

$$\mathcal{I}_{\text{EE}}(A : B) = \mathcal{I}_{\text{EE}}(A^c : B^c), \quad (\text{I.14})$$

This result follows from the invariance of entropy under complement, explicitly, $S_{\text{EE}}(A) = S_{\text{EE}}(A^c)$. Therefore, the SSA condition is also preserved under the simultaneous complement.

For convenience, we introduce a family of quantities akin to the conditional mutual information:

$$\mathcal{I}_f(A : B) = f(A) + f(B) - f(A \cup B) - f(A \cap B) \quad (\text{I.15})$$

which measures the additional quantity beyond the description of the Venn diagram. For example, if we take $f = S_{\text{TEE}}$, then we have the topological conditional mutual information $\mathcal{I}_{\text{TEE}}(A : B)$. We will show that such quantity is also non-negative, i.e., the TEE also satisfies the SSA. In Sec. III and Sec. IV, we will take f to be the intrinsic TEE S_{iTEE} and the genus g , where we will show the modified SSA for the intrinsic TEE

$$\mathcal{I}_{\text{iTEE}}(A : B) \geq 2\mathcal{I}_g(A : B) \ln \mathcal{D}. \quad (\text{I.16})$$

Furthermore, if a function f satisfies $f(A) = f(A^c)$, then $\mathcal{I}_f(A : B)$ is invariant under simultaneous complement of A and B ,

$$\mathcal{I}_f(A^c : B^c) = \mathcal{I}_f(A : B). \quad (\text{I.17})$$

For example, entropies such as the EE, TEE and iTEE all satisfy this property.

B. Generalized surgery

In this section, we briefly review the surgery method introduced by Witten in [7] and present a natural generalization to the method. Consider two three dimensional closed manifolds \tilde{M}_1 and \tilde{M}_2 . By removing a 3-ball D^3 from each manifold, we obtain manifolds M_1 and M_2 respectively. After this removal, both M_1 and M_2 acquire boundaries that are 2-spheres S^2 . The partition function of M_1 and M_2 generate quantum states $|M_1\rangle, |M_2\rangle$ of the Hilbert space \mathcal{H}_{S^2} , which is associated with the S^2 boundary.

Next, we glue the manifolds M_1 and M_2 along their common S^2 boundary, resulting in a new manifold $M = M_1 \cup_{S^2} M_2 = \tilde{M}_1 \# \tilde{M}_2$, which is the connected sum of \tilde{M}_1 and \tilde{M}_2 . The partition function of M can be computed as the inner product $\langle M_1 | M_2 \rangle$ of the two states.

To evaluate this partition function, we insert a complete basis of states for the Hilbert space \mathcal{H}_{S^2} . Since \mathcal{H}_{S^2} is spanned by the single state $|D^3\rangle$, which correspond to the partition function of the 3-ball, we can express the partition function of M as

$$Z(M) = \langle M_1 | M_2 \rangle = \frac{\langle M_1 | D^3 \rangle \langle D^3 | M_2 \rangle}{\langle D^3 | D^3 \rangle}. \quad (\text{I.18})$$

The term $\langle M_i | D^3 \rangle = \langle D^3 | M_i \rangle = Z(\tilde{M}_i)$ represents the partition function of the manifold $M_i \cup_{S^2} D^3 \simeq \tilde{M}_i$. Similarly, $\langle D^3 | D^3 \rangle = Z(S^3)$ is the partition function of $D^3 \cup_{S^2} D^3 = S^3$. Therefore, we can rewrite Eq. (I.18) as

$$Z(M)Z(S^3) = Z(\tilde{M}_1)Z(\tilde{M}_2). \quad (\text{I.19})$$

The surgery method has been extended to include cases where the boundary is S^2 with two marked points a, \bar{a} (see [28] for example). In this case, the Hilbert space is still one-dimensional, i.e., $\dim \mathcal{H}_{S^2, a, \bar{a}} = 1$. However, the surgery method can be generalized to situations where the Hilbert space of the cut is not one-dimensional.

Consider a three manifold M , potentially containing complicated Wilson lines in the bulk. We make an arbitrary cut along a two-dimensional manifold $\Sigma \subset M$, separating M into two submanifolds, M_1 and M_2 . The cut may also intersect the Wilson lines, creating marked points $\{a_i\}_i$ on Σ .

The partition functions of \bar{M}_1, M_2 generate states $|M_1\rangle, |M_2\rangle \in \mathcal{H}_{\Sigma, \{a_i\}}$, and the partition function of M is given by the inner product $Z(M) = \langle M_1 | M_2 \rangle$. To evaluate this inner product, we insert a complete orthogonal basis β of $\mathcal{H}_{\Sigma, \{a_i\}}$, yielding:

$$Z(M) = \langle M_1 | M_2 \rangle = \sum_{v \in \beta} \frac{\langle M_1 | v \rangle \langle v | M_2 \rangle}{\langle v | v \rangle}. \quad (\text{I.20})$$

In particular, when $\Sigma = S^2$, the Hilbert space $\mathcal{H}_{\Sigma, \{a_i\}}$ can be spanned by a fusion tree basis $V_{\{a_i\}}$ (See Sec. III C for concrete examples).

II. Classification of bipartitions

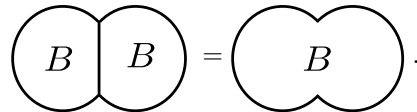
A. Regularization of bipartitions

To analyze the topology of our subregions more carefully, we need to pay close attention to whether a subregion includes its boundary points.

Typically, we think of subregions as open subsets. However, when considering a bipartition of a torus $T^2 = A \cup B$, the situation is more nuanced. It is impossible for two open sets to disjointly cover a closed manifold like the torus. Therefore, the appropriate condition for A, B to form a bipartition of T^2 is that $\bar{A} \cup B = T^2$, where \bar{A} is the closure of A , and their boundaries coincide, i.e. $\partial A = \partial B$, with ∂ denoting the boundary. For simplicity, we will continue to use the notation $T^2 = A \cup B$ throughout this paper.

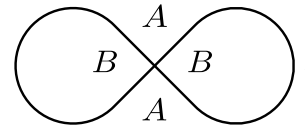
In this context, constructing the reduced density matrix ρ_A introduces an ambiguity: we must decide whether to glue the manifolds along B or its closure \bar{B} . For instance, consider the case where B consists of two disjoint open disks whose boundaries intersect at a line segment. In this situation, it is natural to treat these two disks as part of a single connected component, meaning we glue

along their boundaries. This is illustrated as follows:

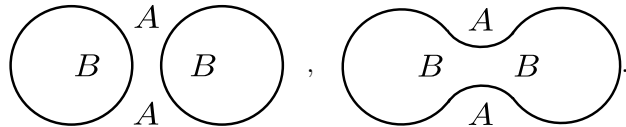


In this situation, the ambiguity can be resolved.

However, the situation becomes problematic when A and B intersect at a point rather than along a line segment, such as in the case of a tetrajunction. For example, consider the following bipartition on S^2



This configuration is the limiting case between two distinct situations:



The TEE for the left configuration is $-2 \ln \mathcal{D}$, while for the right one it is $-\ln \mathcal{D}$. Therefore, the limiting case with the tetrajunction is ill-defined in the context of TQFT. Physically, as the length scale near the junction shrinks towards zero, it becomes smaller than the correlation length of the ultraviolet (UV) theory, meaning that the TQFT is no longer a valid approximation for the underlying UV theory. We suspect that there may be a necessary corner contribution in such cases, which complicates the calculation of TEE.

To avoid these subtleties, we will focus on configurations where no such junctions occur. More specifically, we require that the boundaries of different connected components remain disjoint. With this physical consideration, the gluing of subregions becomes well-defined by gluing the closure of the subregions. Consequently, we can consistently compute the TEE within the TQFT framework.

B. Classification of bipartitions

We now classify the bipartitions of a torus based on their entanglement interfaces. These interfaces are composed of disjoint loops, which we categorize by the types of loops present. On a torus, each loop is either a torus knot or a contractible loop.

Let $K(p, q)$ be the torus knot that winds $p \in \mathbb{Z}$ times around the meridian and $q \in \mathbb{Z}$ times around the longitude. To prevent the knot from self-intersecting, we require that p and q be co-prime, meaning $\gcd(p, q) = 1$. If the entanglement interface contains two different types of non-contractible torus knots (i.e., knots where at least one of p or q is different), these knots will necessarily intersect. Thus, the entanglement interfaces we consider

can only include one type of non-contractible torus knot, along with possibly some contractible loops.

Furthermore, any non-contractible torus knots must appear in pairs, as this is necessary for them to properly divide the torus into two distinct regions. Thus, the general form of the entanglement interface can be expressed as follows:

$$\partial A = \partial B = (\amalg_{i=1}^n C_i) \amalg (\amalg_{j=1}^{2m} K_j(p, q)), \quad (\text{II.1})$$

where the C_i 's represent contractible loops, $K_j(p, q) \simeq K(p, q)$ are non-intersecting torus knots of the same p, q , and $m, n \in \mathbb{Z}$ are integers.

C. Canonical bipartitions on a torus

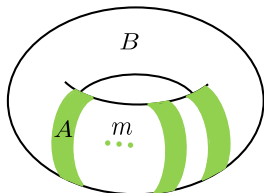


FIG. 1. A canonical bipartition of m rings.

We define a bipartition on the torus T^2 as a canonical bipartition R_m if its entanglement interface consists solely of $2m$ meridians, i.e.,

$$R_m = \amalg_{j=1}^{2m} K_j(1, 0), \quad (\text{II.2})$$

where we called m the number of rings. In this section, we will establish a connection between the TEE for an arbitrary bipartition and that of a canonical bipartition. This connection will be made by systematically removing contractible loops (referred to as "bubbles") and applying appropriate coordinate transformations. An illustrative example of this process can be found in Fig. 2.

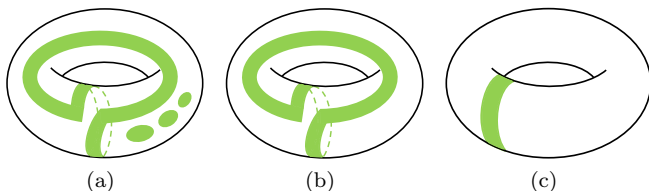


FIG. 2. An example of transforming a general bipartition into a canonical bipartition proceeds as follows: by removing the three contractible loops in (a), we obtain the configuration shown in (b), where the entanglement interface consists of two $K(1, 1)$ knots. We then apply a coordinate transformation to this interface, converting the two $K(1, 1)$ knots into two meridian loops. This transformation results in the canonical R_1 bipartition, as depicted in (c).

Consider a vacuum state on the torus T^2 , generated by a solid torus [29] with the bipartition $T^2 = A \cup B$.

The subregion A can be divided into two disjoint parts, $A = A_1 \amalg A_2$. Suppose that A_2 is contractible on T^2 , there exist a circle $S^1 \subset T^2$ that encloses A_2 , separating B into B_1 and B_2 . We now extend such S^1 interface into a disk D^2 inside the bulk [30], which separates the solid torus into two components: $M_1 \simeq D^2 \times S^1$ and $M_2 \simeq D^3$ (See Fig. 3). In this setup, the original solid torus $M \simeq D^2 \times S^1$ can be viewed as the gluing of M_1 and M_2 along the common boundary D^2 , i.e. $M = M_1 \cup_{D^2} M_2$.

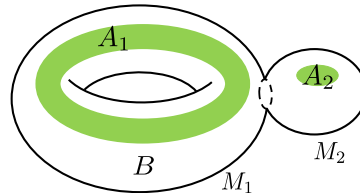


FIG. 3. In this diagram, A_1 is represented by a non-contractible annulus, while A_2 corresponds to a disk. The dashed line indicates the S^1 boundary, and the disk bounded by the S^1 separates the solid torus into the left part M_1 and the right part M_2 .

Next, we can construct the reduced density matrix by gluing the manifold with its orientation-reversed counterpart. The two boundaries D^2 are glued to become a S^2 separating the glued manifold into two parts: $\rho_A = \tilde{M}_1 \cup_{S^2} \tilde{M}_2$, where $\tilde{M}_i = M_i \cup_{B_i} \tilde{M}_i$ with $i = 1, 2$. That is, the reduced density matrix becomes a connected sum of \tilde{M}_1 and \tilde{M}_2 . One can apply the surgery method before performing the replica method

$$\rho_A(M) = \frac{\rho_{A_1}(M_1) \otimes \rho_{A_2}(M_2)}{Z(S^3)}. \quad (\text{II.3})$$

Tracing the n -th power of the reduced density matrix, we obtain

$$\text{Tr} \rho_A(M)^n = \frac{\text{Tr}(\rho_{A_1}(M_1))^n \text{Tr}(\rho_{A_2}(M_2))^n}{Z(S^3)^n}. \quad (\text{II.4})$$

In particular, if $A_2 \simeq D^2$, then $\text{Tr}(\rho(M_2, A_2))^n = Z(S^3)$ and hence the TEE is given by

$$\begin{aligned} S(M, A) &= \lim_{n \rightarrow 1} \frac{1}{1-n} \ln(\rho(M_1, A_1))^n \\ &\quad + \lim_{n \rightarrow 1} \frac{1}{1-n} \ln Z(S^3)^{1-n} \\ &= S(M_1, A_1) - \ln \mathcal{D} \end{aligned} \quad (\text{II.5})$$

Thus, when computing the TEE, we can effectively remove an isolated D^2 subregion—referred to as a "bubble"—by adding back $-\ln \mathcal{D}$ to the final result. For ex-

ample,

$$S_{\text{TEE}} \left(\begin{array}{c} \text{A} \\ \text{B} \end{array} \right) = S_{\text{TEE}} \left(\begin{array}{c} \text{A} \\ \text{B} \end{array} \right) - \ln \mathcal{D}. \quad (\text{II.6})$$

In general, if A_2 is a contractible region on the torus and $A_1 \cap A_2 = \emptyset$, then we have

$$S_{\text{TEE}}(T^2, A) = S_{\text{TEE}}(T^2, A_1) + S_{\text{TEE}}(S^3, A_2). \quad (\text{II.7})$$

There is also another type of bubble where the isolated D^2 subregion is located within A rather than B . In this scenario, we can leverage the fact that the TEE is identical for a subregion A and its complement B . By interchanging the roles of A and B , the second type of bubble effectively transforms into the first type of bubble. Consequently, we can remove this bubble by adding $-\ln \mathcal{D}$ to the TEE. For example,

$$S_{\text{TEE}} \left(\begin{array}{c} \text{A} \\ \text{B} \end{array} \right) = S_{\text{TEE}} \left(\begin{array}{c} \text{A} \\ \text{B} \end{array} \right) - \ln \mathcal{D}. \quad (\text{II.8})$$

Finally, by induction, we can remove all contractible interfaces between the subregions by adding an integer multiple of $-\ln \mathcal{D}$. More explicitly, for a general bipartition represented by Eq. (II.1), we have

$$S_{\text{TEE}}((\Pi_{i=1}^n C_i) \amalg (\Pi_{j=1}^{2m} K_j(p, q))) = S_{\text{TEE}}(\Pi_{j=1}^{2m} K_j(p, q)) - n \ln \mathcal{D}. \quad (\text{II.9})$$

Therefore, it remains to compute the TEE for a bipartition whose interface consists of $2m$ copies of torus knots.

In Ref. [31], we demonstrated that a state with a torus knot bipartition can be mapped to an effective state with a meridian bipartition. In fact, the same mapping can be applied to a bipartition consisting of multiple torus knots. Let $|\psi\rangle = \sum_a \psi_a |a\rangle$ represent the original state, and let

\mathcal{O} be the transformation that maps the torus knots back to the meridian. Then, we have:

$$S(|\psi\rangle, \Pi_{j=1}^{2m} K_j(p, q)) = S(|\mathcal{O}\psi\rangle, R_m), \quad (\text{II.10})$$

where $|\mathcal{O}\psi\rangle = \sum_{a,b} \mathcal{O}_{ab} \psi_b |a\rangle$. Therefore, we can study the TEE for any bipartition by examining the TEE for canonical bipartitions with Wilson lines inserted in the bulk.

III. The intrinsic TEE and TEE for general bipartitions

A. The intrinsic TEE and the topological RT formula

For a canonical bipartition of a single ring, it has been established that the TEE is bounded [21, 31] by

$$-2 \ln \mathcal{D} \leq S_{\text{TEE}} \leq 0. \quad (\text{III.1})$$

In this paper, we will demonstrate that, in general, for any bipartition on a torus, the TEE possesses a lower bound that can always be saturated. We define this minimal TEE as the intrinsic TEE for a subregion A

$$S_{i\text{TEE}}(A) = \min_{|\psi\rangle \in \mathcal{H}} S_{\text{TEE}}(A, |\psi\rangle). \quad (\text{III.2})$$

Due to the results of Eq. (II.9) and Eq. (II.10), for a generic state $|\psi\rangle = \sum_a \psi_a |a\rangle$ and a generic bipartition $(\Pi_{i=1}^n C_i) \amalg (\Pi_{j=1}^{2m} K_j(p, q))$, the TEE is given by:

$$S_{\text{TEE}}(|\psi\rangle, (\Pi_{i=1}^n C_i) \amalg (\Pi_{j=1}^{2m} K_j(p, q))) = -n \ln \mathcal{D} + S_{\text{TEE}}(|\mathcal{O}\psi\rangle, R_m). \quad (\text{III.3})$$

Intuitively, Wilson lines serve as links between the rings, thereby increasing the entanglement. Consequently, we expect that the minimal TEE is achieved when there are no Wilson lines, i.e., when $|\mathcal{O}\psi\rangle = |0\rangle$. This can be achieved by taking $|\psi\rangle = \sum_a \mathcal{O}_{a0}^{-1} |a\rangle$.

Although intuitively simple, the proof that we will demonstrate Sec. III B is more involved. For the vacuum state with a canonical bipartition consisting of m rings, we will show in Sec. III B that the TEE is simply given by

$$S_{\text{TEE}}(|0\rangle, R_m) = -2m \ln \mathcal{D}. \quad (\text{III.4})$$

Therefore, the intrinsic TEE for a generic state and bipartition on a torus is given by

$$S_{i\text{TEE}}(|\psi\rangle, (\Pi_{i=1}^n C_i) \amalg (\Pi_{j=1}^{2m} K_j(p, q))) = -(n+2m) \ln \mathcal{D}. \quad (\text{III.5})$$

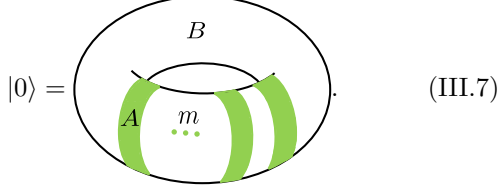
Interestingly, $n+2m = |\pi_0(\partial A)| := \pi_{\partial A}$ represents the number of loops in the interface. This indicates that the intrinsic TEE is a purely topological quantity.

B. Vacuum state

As a warm-up, we first demonstrate that by applying the replica and surgery method, the TEE for the vacuum state with the canonical bipartition of m rings is given by:

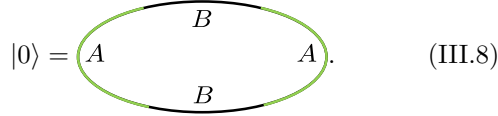
$$S_{\text{TEE}}(|0\rangle, R_m) = -2m \ln \mathcal{D}. \quad (\text{III.6})$$

Consider a vacuum state with the R_m bipartition, represented as follows:



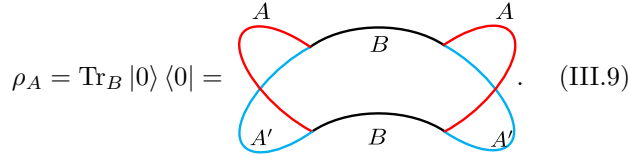
$$|0\rangle = \text{Diagram} \quad (\text{III.7})$$

For simplicity of visualization, let us consider the case where $m = 2$. We also contract our solid torus into a circle, where each point represents a D^2



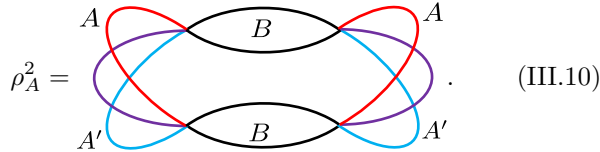
$$|0\rangle = \text{Diagram} \quad (\text{III.8})$$

The reduced density matrix is obtained by adding an orientation reversed copy of $|0\rangle$ and gluing them together along the B subregion:



$$\rho_A = \text{Tr}_B |0\rangle \langle 0| = \text{Diagram} \quad (\text{III.9})$$

In the diagram, we use different colors to differentiate the subregions of the two copies, facilitating identification during the gluing process. Each point on the B regions (indicated by black lines) now represents an S^2 , while each point in the A, A' regions (indicated by red and blue lines) continues to represent a D^2 . To compute ρ_A^2 , we simply add another copy of ρ_A and glue the red region of the first copy to the blue region of the second copy:

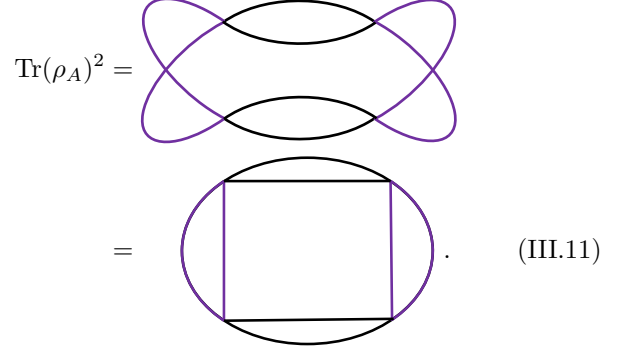


$$\rho_A^2 = \text{Diagram} \quad (\text{III.10})$$

In this representation, the purple regions indicate where the red and blue regions are glued together. Consequently, each point on the purple region represents an S^2 .

Finally, taking trace of ρ_A^2 corresponds to gluing the

remaining red and blue regions together:



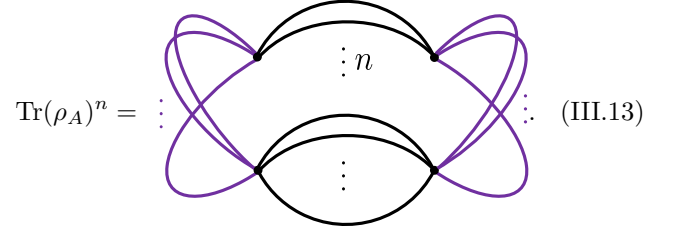
$$\text{Tr}(\rho_A)^2 = \text{Diagram} \quad (\text{III.11})$$

In the second figure, we place everything onto a plane. Now that all the boundaries are properly glued, each point (both purple and black) in this configuration represents an S^2 . Therefore, the configuration is a connected sum of five copies of $S^2 \times S^1$'s. To evaluate the partition function of such a configuration, we perform the surgery method by inserting four copies of S^3 to separate the $S^2 \times S^1$ components:

$$\text{Tr}(\rho_A)^2 = \frac{Z(S^2 \times S^1)^5}{Z(S^3)^4} = \mathcal{D}^4, \quad (\text{III.12})$$

where we use the fact that $Z(S^2 \times S^1) = 1$ and $Z(S^3) = \mathcal{D}^{-1}$ (see [7]).

In general, for $\text{Tr}(\rho_A)^n$, we will have n lines connecting each neighboring pair of nodes:



$$\text{Tr}(\rho_A)^n = \text{Diagram} \quad (\text{III.13})$$

This figure consist of $4(n-1) + 1$ holes[32], which form a connected sum of $4(n-1) + 1$ copies of $S^2 \times S^1$. Therefore, we can perform the surgery by inserting $4(n-1)$ copies of S^3 to separate the configuration:

$$\text{Tr}(\rho_A)^n = \frac{Z(S^2 \times S^1)^{4(n-1)+1}}{Z(S^3)^{4(n-1)}} = \mathcal{D}^{4(n-1)}. \quad (\text{III.14})$$

The TEE is then given by:

$$S_{\text{TEE}}(|0\rangle, R_2) = \lim_{n \rightarrow 1} \frac{1}{1-n} \ln \text{Tr}(\rho_A)^n = -4 \ln \mathcal{D}. \quad (\text{III.15})$$

For general R_m bipartition, the configuration of $\text{Tr}(\rho_A)^n$ consists of $2m$ nodes, with n lines connecting neighboring nodes. As a result, the configuration forms a connected sum of $2m(n-1) + 1$ copies of $S^2 \times S^1$. The partition function is evaluated by inserting $2m(n-1)$ copies of S^3 to separate the components. Thus, we have:

$$\text{Tr}(\rho_A)^n = \mathcal{D}^{2m(n-1)}. \quad (\text{III.16})$$

detailed review), one can verify that this basis is indeed orthogonal, with normalization:

$$\langle e, \mu, \nu | f, \alpha, \beta \rangle = e \mathbf{f} = \delta_{ef} \delta_{\mu\alpha} \delta_{\nu\beta} \frac{d_b d_d}{\mathcal{D}}. \quad (\text{III.23})$$

We apply the generalized surgery by inserting the complete orthonormal basis:

$$\langle L | R \rangle = \sum_{e, \mu, \nu} \frac{\langle L | e, \mu, \nu \rangle \langle e, \mu, \nu | R \rangle}{\langle e, \mu, \nu | e, \mu, \nu \rangle}. \quad (\text{III.24})$$

Pictorially, this is represented by:

$$= \sum_{e, \mu, \nu} \frac{\mathcal{D}}{d_b d_d} \text{Diagram} \quad (\text{III.25})$$

For the right diagram in the equation, we evaluate it using the bubble merging diagram. This simplifies to:

$$\langle e, \mu, \nu | R \rangle = \text{Diagram} = \sqrt{\frac{d_b d_d}{d_e}} \delta_{0e} \delta_{\mu, \nu}. \quad (\text{III.26})$$

Thus, the sum over e collapses due to δ_{0e} , leaving us with:

$$\text{Diagram} = \sum_{\mu, \nu} \frac{\mathcal{D}}{\sqrt{d_b d_d}} \text{Diagram} \quad (\text{III.27})$$

Following the process, we next cut off the left hole in the diagram. Applying the same surgery method as before, we obtain:

$$\text{Diagram} = \sum_{\mu', \nu'} \frac{\mathcal{D}}{\sqrt{d_b d_d}} \text{Diagram} \quad (\text{III.28})$$

This step introduces an additional constraint: $b = d$. Therefore, the indices μ, ν, μ', ν' can be neglected since there's a unique channel for an anyone to merge with its inverse.

Finally, we apply the surgery method twice more to separate all three holes:

$$\begin{aligned} \text{Diagram} &= \left(\frac{\mathcal{D}}{d_c}\right)^2 \left(\text{Diagram}\right)^2 \left(\text{Diagram}\right) \\ &= \left(\frac{\mathcal{D}}{d_c}\right)^2 \delta_{bc} \delta_{ac}. \end{aligned} \quad (\text{III.29})$$

Combining the above results, we have:

$$\text{Tr}(\rho_A)^2 = \sum_a |\psi_a|^4 \left(\frac{\mathcal{D}}{d_a}\right)^4. \quad (\text{III.30})$$

Next, we consider the case of $\text{Tr}(\rho_A)^3$. In this configuration, we have four nodes arranged in a circle, with each neighboring pair connected by three lines. If we label the leaves from inside to outside as 1, 2, 3, the possible labels for the Wilson lines can be represented as: 1111, 1212, 2222, 2323, 3333, 3131. Notably, because the even labels are identical to each other and the odd labels are also identical, we can simplify our labeling. For example, we can denote the Wilson lines by their even and odd labels rather than writing out each full label explicitly.

To visualize the configuration, we can represent it as follows:

$$\text{Tr}(\rho_A)^3 = \sum_{\substack{a_{11}, a_{12}, a_{22}, \\ a_{23}, a_{33}, a_{31}}} \psi_{11} \bar{\psi}_{12} \psi_{22} \bar{\psi}_{23} \psi_{33} \bar{\psi}_{31} \quad (III.31)$$

To make the induction pattern clearer, we can exchange the rows of the diagram such that the internal rows are arranged in decreasing order from inside to outside, except for the outermost one:

$$\quad (III.32)$$

This adjustment helps to visualize the similarity between the configurations in each layer.

By applying the surgery method to the left and right-most holes as detailed in Eq. (III.27) and Eq. (III.28), we then obtain

$$\quad (III.33)$$

Next, we proceed to remove the uppermost and lower-

most holes, resulting in:

$$\quad (III.34)$$

Finally, we rename the row indices to achieve a configuration equivalent to $\text{Tr}(\rho_A)^2$. Therefore, from Eq. (III.27), Eq. (III.28) and Eq. (III.29), we have

$$\quad (III.35)$$

Combining these results, we arrive at the expression:

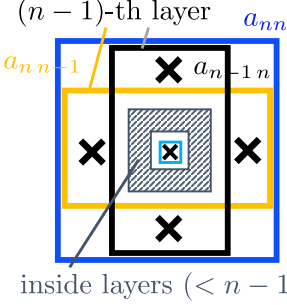
$$\text{Tr}(\rho_A)^3 = \sum_a |\psi_a|^6 \left(\frac{\mathcal{D}}{d_a}\right)^8. \quad (III.36)$$

In general, for $\text{Tr}(\rho_A)^n$, we have $n - 1$ layers. Each layer consists of 4 holes positioned on the left, right, top, and bottom. Including the hole in the center, this gives a total of $4(n - 1) + 1$ holes, as discussed in Sec. III B

$$\text{Tr}(\rho_A)^n = \quad (III.37)$$

By applying the surgery method to the outermost layer

of holes, we obtain the configuration for $\text{Tr}(\rho_A)^{n-1}$



(n-1)-th layer a_{nn}

$a_{n,n-1}$

inside layers (< n-1)

$$= \left(\frac{D}{d_\bullet}\right)^4 \delta_{\bullet\bullet\bullet\bullet} \delta_{\bullet\bullet\bullet\bullet} \delta_{\bullet\bullet\bullet\bullet} \delta_{\bullet\bullet\bullet\bullet}, \quad (\text{III.38})$$

a_{nn}

inside layers (< n-1)

where we use the colored dots to label the Wilson lines and the delta functions constrain all the outer layer Wilson lines to be identical. By induction, we perform surgery for a total of $n-1$ layers, resulting in a cumulative contribution of $-4(n-1)$ th power of S_{0a} . Thus, the overall result is:

$$\text{Tr}(\rho_A)^n = \sum_a |\psi_a|^{2n} \left(\frac{D}{d_a}\right)^{4(n-1)}. \quad (\text{III.39})$$

The TEE is then given by:

$$\begin{aligned} S_{\text{TEE}} &= \lim_{n \rightarrow 1} \frac{1}{1-n} \ln \text{Tr}(\rho_A)^n \\ &= \sum_a 2|\psi_a|^2 (2 \ln d_a - \ln |\psi_a|) - 4 \ln \mathcal{D}. \end{aligned} \quad (\text{III.40})$$

To find the minimum under the constraints $0 \leq |\psi_a| \leq 1$ and $\sum_a |\psi_a|^2 = 1$, we consider that the minimum must occur at a local extremum or on the boundary of the feasible region. Utilizing the method of Lagrange multipliers, as discussed in [31], we determine that the global minimum is attained at the boundary when $|\psi_a| = \delta_{0a}$.

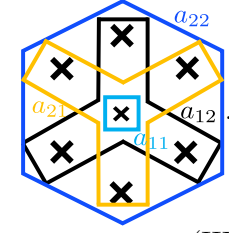
This minimum corresponds to the scenario where no Wilson lines are inserted into the bulk. This aligns with our intuition that Wilson lines act as entangled pairs of quasi-particles across subregions, thereby increasing the overall entanglement.

Consequently, we complete the proof for the special case where $m=2$ in the previous section, showing that the intrinsic topological entanglement entropy (TEE) for a canonical R_2 bipartition is given by $-4 \ln \mathcal{D}$.

D. Generic state on R_3 and R_m bipartition

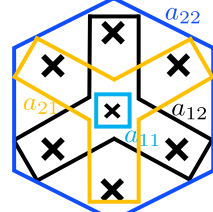
Before generalizing the result to arbitrary rings, we will first examine the R_3 bipartition. Consider a generic state $|\psi\rangle = \sum_a \psi_a |a\rangle$ with the R_3 bipartition. The bulk configuration for $\text{Tr}(\rho_A)^2$ now consists of six nodes arranged in a circle, with each neighboring pair connected by two

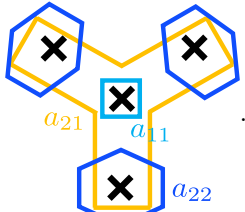
lines. Using similar pictorial notation as in the previous section, we have

$$\begin{aligned} \text{Tr}(\rho_A)^2 &= \sum_{a_{11}, a_{12}, a_{22}, a_{21}} \psi_{11} \bar{\psi}_{12} \psi_{22} \bar{\psi}_{21} \end{aligned}$$


(III.41)

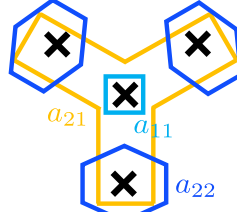
In the figure, there are six rows of holes oriented at an angle of $\frac{n\pi}{3}$, where $n=0, 1, \dots, 5$. We separate these rows into two groups based on whether n is even or odd. We denote a Wilson loop a_{ij} if it threads through the i -th layer on the even rows and j -th layer on the odd rows. We apply the surgery method to the outermost holes of the even rows, resulting in



$$= \left(\frac{D}{d_{22}}\right)^3 \delta_{a_{22}, a_{12}}$$


(III.42)

Next, we perform the surgery on the outermost holes of the odd rows:



$$= \left(\frac{D}{d_{22}}\right)^3 \delta_{a_{22}, a_{21}} \delta_{a_{22}, a_{11}}.$$

(III.43)

Combining the results, we obtain

$$\text{Tr}(\rho_A)^2 = \sum_a |\psi_a|^4 \left(\frac{D}{d_a}\right)^6. \quad (\text{III.44})$$

For $\text{Tr}(\rho_A)^n$, the bulk configuration consists of six nodes with n lines connecting neighboring nodes. This configuration translates to a figure with $n-1$ layers of holes, where each layer consists of six holes. We then repeat the surgery method on the even and odd rows, layer

by layer, obtaining

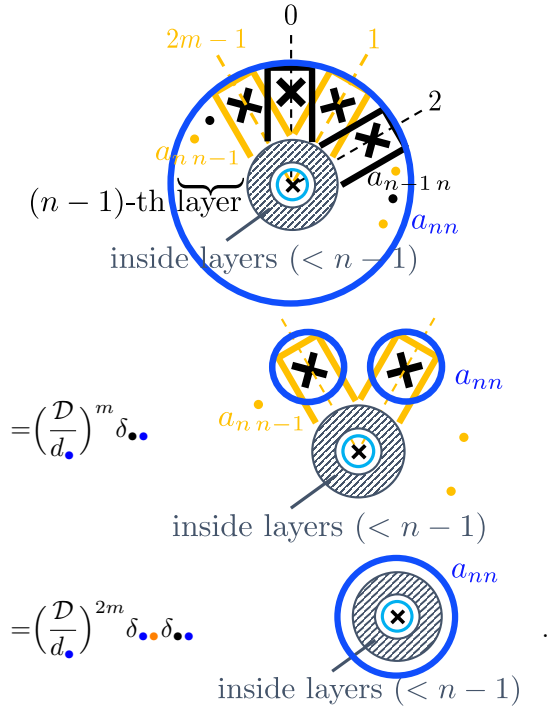
$$\text{Tr}(\rho_A)^n = \sum_a |\psi_a|^{2n} \left(\frac{\mathcal{D}}{d_a}\right)^{6(n-1)}. \quad (\text{III.45})$$

The TEE is therefore given by

$$S_{\text{TEE}} = \sum_a 2|\psi_a|^2 (3 \ln d_a - \ln |\psi_a|) - 6 \ln \mathcal{D}, \quad (\text{III.46})$$

which reaches its minimum value of $-6 \ln \mathcal{D}$ when there are no Wilson lines present.

Similar arguments can be generalized to the R_m bipartition. In this case, the configuration will consist of $2m$ rows of holes, which can be separated into even and odd rows. Surgery method is then applied layer by layer to the $n-1$ layers of holes. For each layer, we perform the surgery on the even and odd rows sequentially to remove the $2m$ holes:



By induction, after peeling off all $n-1$ layers, we obtain

$$\text{Tr}(\rho_A)^n = \sum_a |\psi_a|^{2n} \left(\frac{\mathcal{D}}{d_a}\right)^{2m(n-1)}. \quad (\text{III.47})$$

The TEE is then given by

$$S_{\text{TEE}} = \sum_a p_a (m \ln d_a - \ln p_a) + -2m \ln \mathcal{D}, \quad (\text{III.48})$$

where $p_a = |\psi_a|^2$ plays the role of classical probability.

The topological entanglement entropy (TEE) can be separated into three distinct components:

1. **Intrinsic TEE** $S_{\text{iTEE}} = -2m \ln \mathcal{D}$: This is a non-positive contribution that depends solely on the number of interfaces between the two subregions of the system. It does not depend on any specific ground state configuration.

2. **Wilson line** contribution $S_{\text{Wil}} = 2m \sum_a p_a \ln d_a$: This term represents a non-negative contribution to the entanglement due to the presence of Wilson lines linking the two subregions. The linkage between subregions is proportional to the number of non-contractible interfaces and contributes to the total entanglement through the quantum dimensions d_a of different quasi-particle types.

3. **Classical** contribution $S_{\text{cl}} = -2 \sum_a p_a \ln p_a$: This non-negative contribution arises from the classical superposition of degenerate ground states. The term is directly related to the Shannon entropy of the ground state probabilities. Importantly, this classical contribution only manifests when the bipartition of the system encloses a non-contractible loop, meaning that the system's topology plays a critical role in its appearance.

The latter two contributions, S_{Wil} and S_{cl} both arise due to the degeneracy of the ground state in a topologically ordered system. These contributions reflect entanglement properties that depend on the specific ground state configuration.

We refer to the combination of these two contributions as the ground state TEE:

$$S_{\text{gs}} = S_{\text{Wil}} + S_{\text{cl}} = \sum_a p_a (m \ln d_a - \ln p_a) \geq 0. \quad (\text{III.49})$$

This ground state TEE is always non-negative and only appears when $m > 1$, meaning that the bipartition of the system winds around a non-contractible cycle on the torus.

In summary, given a general bipartition of a torus with boundary $\partial A = (\prod_{i=1}^n C_i) \amalg (\prod_{j=1}^{2m} K_j(p, q))$, the bipartition can be simplified to the canonical form R_m . This is done by removing the contractible interfaces, which introduces a correction term $-n \ln \mathcal{D}$, and applying a coordinate transformation that maps the original state $|\psi\rangle$ to an effective state $|\mathcal{O}\psi\rangle$. The resulting TEE is:

$$S_{\text{TEE}}(A, |\psi\rangle) = S_{\text{TEE}}(R_m, |\mathcal{O}\psi\rangle) - n \ln \mathcal{D}. \quad (\text{III.50})$$

The TEE for the R_m bipartition can be further decomposed as:

$$S_{\text{TEE}}(R_m, |\psi\rangle) = -2m \ln \mathcal{D} + S_{\text{gs}}(R_m, |\psi\rangle). \quad (\text{III.51})$$

The intrinsic TEE of A is given by

$$S_{\text{iTEE}}(A) = -\pi_{\partial A} \ln \mathcal{D}. \quad (\text{III.52})$$

where $\pi_{\partial A} = 2m + n$ represents the number of interface components (contractible and non-contractible). The intrinsic TEE also serves as the lower bound for the TEE. As a side note, these results can also be derived using the edge state approach, which is discussed in App. C.

IV. The modified SSA of S_{ITEE}

In Sec. III, we have established that the intrinsic TEE is a purely topological quantity given by $S_{\text{ITEE}}(A) = -\pi_{\partial A} \ln \mathcal{D}$, which depends only on the number of connected components of the boundary ∂A . In this section, we will use topological arguments to demonstrate that the intrinsic TEE satisfies a modified version of the strong subadditivity (SSA):

$$\mathcal{I}_{\text{ITEE}}(A : B) \geq -2\mathcal{I}_{\text{g}}(A : B) \ln \mathcal{D}, \quad (\text{IV.1})$$

where

$$\begin{aligned} \mathcal{I}_{\text{ITEE}}(A : B) &:= S_{\text{ITEE}}(A) + S_{\text{ITEE}}(B) - S_{\text{ITEE}}(A \cup B) \\ &\quad - S_{\text{ITEE}}(A \cap B), \\ \mathcal{I}_{\text{g}}(A : B) &:= g_A + g_B - g_{A \cup B} - g_{A \cap B}, \end{aligned} \quad (\text{IV.2})$$

with g_X representing the genus of surfaces X with boundary, as will be discussed later.

We have previously discussed that the boundary of any subregion A can be expressed as in Eq. (II.1). The subregion A can be decomposed into its connected components, $A = \Pi_{i=1}^{\pi_A} A_i$, where each A_i is a connected component, and π_A represents the number of these connected components.

These connected components are compact, connected surfaces, which can be obtained by adding $\pi_{\partial A}$ punctures to a compact surface without boundary of genus g_X . The Euler characteristic of such a surface is given by

$$\chi_X = 2 - 2g_X - \pi_{\partial X}, \quad (\text{IV.3})$$

where $\pi_{\partial X}$ denotes the number of connected components of the boundary ∂X .

Next, we classify the connected components of a subregion on a torus. There are three possible types of connected components on a torus, depending on the number of torus cycles they contain:

1. **Punctured disk:** This is the case where the connected component contains no torus cycles. It can be obtained by puncturing a sphere S^2 , giving it a genus $g_{A_i} = 0$.
2. **Punctured ribbon:** The connected component contains one type of non-contractible torus knot $K(p, q)$. Its boundary consists of two such $K(p, q)$ knots along with multiple contractible loops. This surface also has a genus $g_{A_i} = 0$, as it can be derived from puncturing a sphere.
3. **Punctured torus:** The connected component contains all torus cycles, representing a full torus with punctures. This gives the surface a genus $g_{A_i} = 1$, corresponding to the genus of T^2 .

Now that we have determined the genus for each connected component A_i , the genus for the entire subregion

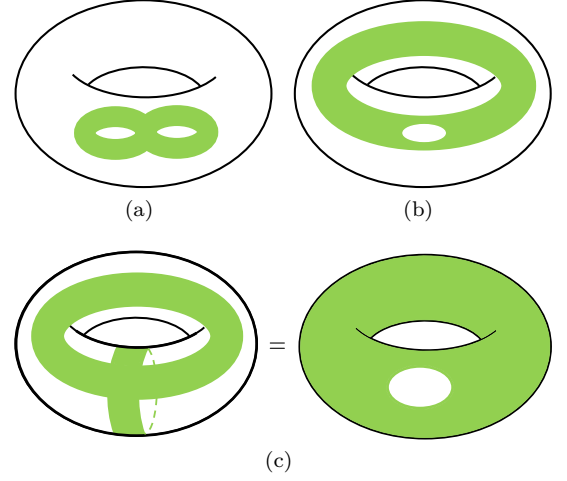


FIG. 4. The green region A on each torus illustrates the three possible connected components: (a) a punctured disk component ($g_A = 0$), (b) a punctured ribbon component ($g_A = 0$), and (c) a punctured torus component ($g_A = 1$).

A is simply the sum of the g_{A_i} 's

$$2g_A = 2 \sum_i g_{A_i} = 2\pi_A - \pi_{\partial A} - \chi_A, \quad (\text{IV.4})$$

where π_A is the number of connected components, $\pi_{\partial A}$ is the number of boundary components, and χ_A is the Euler characteristic of the subregion A .

Moreover, since a punctured torus component must intersect either with a punctured ribbon or another punctured torus, they cannot coexist within the same subregion A . As a result, subregions can be classified into only two types based on the genus: $g_A = 0$ and $g_A = 1$.

Furthermore, suppose $A \subset B$ and $g_A = 1$. In this case, A contains a punctured torus component, which implies that there must be a component of B that also contains this punctured torus component. Therefore, we have $g_B = 1 \geq g_A$. This leads to the following monotonicity property:

$$g_A \leq g_B \text{ if } A \subset B. \quad (\text{IV.5})$$

Since $A \subset A \cup B$ and $A \cap B \subset B$, by Eq. (IV.5) we have $g_A \leq g_{A \cup B}$ and $g_{A \cap B} \leq g_B$. Therefore, we obtain the following bounds

$$-1 \leq \mathcal{I}_{\text{g}}(A : B) \leq 1. \quad (\text{IV.6})$$

This implies that the modification of the SSA for the intrinsic TEE (Eq. (IV.1)) is at most $2 \ln \mathcal{D}$.

Now that we have expressed the number of boundary components in terms of the number of connected components and the Euler characteristic, we can leverage our understanding of topology to explore relationships related to the SSA.

Let $A = \Pi_{i=1}^{\pi_A} A_i$, $B = \Pi_{i=1}^{\pi_B} B_i$ represent the decompositions of A, B into their connected components. We

can construct a graph where the nodes correspond to the A_i and B_i components. We draw n edges between A_i and B_j if the intersection $A_i \cap B_j$ contains n connected components.

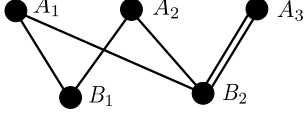


FIG. 5. An example for the relation between A, B subregions.

According to a result in graph theory, for a connected graph, we have:

$$\text{Edges} \geq \text{Vertices} - 1. \quad (\text{IV.7})$$

In our case, the graph consist of $\pi_{A \cup B}$ components. By summing over all these connected graphs gives us:

$$\text{Edges} \geq \text{Vertices} - \pi_{A \cup B}. \quad (\text{IV.8})$$

By identifying the number of vertices as $\pi_A + \pi_B$ and the number of edges as $\pi_{A \cap B}$, we can rewrite the inequality as:

$$\pi_A + \pi_B \leq \pi_{A \cap B} + \pi_{A \cup B}. \quad (\text{IV.9})$$

Using the notation from Eq. (I.15), we can express this as:

$$\mathcal{I}_\pi(A : B) \leq 0. \quad (\text{IV.10})$$

On the other hand, since our ambient space is compact, we can apply the inclusion-exclusion principle for the Euler characteristic, which states that:

$$\chi_A + \chi_B = \chi_{A \cup B} + \chi_{A \cap B}, \quad (\text{IV.11})$$

This means that the Euler characteristic is fully captured by the Venn diagram:

$$\mathcal{I}_\chi(A : B) = 0. \quad (\text{IV.12})$$

Next, we use Eq. (III.52) and apply \mathcal{I} to each term of Eq. (IV.4), leading to the relation:

$$\mathcal{I}_{\text{iTEE}} = -(2\mathcal{I}_\pi - 2\mathcal{I}_g - \mathcal{I}_\chi) \ln \mathcal{D}. \quad (\text{IV.13})$$

By applying Eq. (IV.10) alongside Eq. (IV.12), we obtain the following inequality:

$$\mathcal{I}_{\text{iTEE}} \geq 2\mathcal{I}_g \ln \mathcal{D}. \quad (\text{IV.14})$$

In conclusion, the strong subadditivity of the intrinsic TEE receives a modification due to the presence of \mathcal{I}_g . This modification is mild, as the absolute value of \mathcal{I}_g is bounded by $2 \ln \mathcal{D}$.

V. The SSA of S_{TEE}

Although S_{iTEE} does not always satisfy the SSA condition, it is anticipated that S_{TEE} satisfies the SSA condition for the following reasons. Consider a TQFT realized by the ground states of a lattice model. It is expected that the entanglement entropy of this lattice model can be expressed as [11, 12]:

$$S_{\text{EE}}(A) = \alpha L_A + S_{\text{TEE}}(A). \quad (\text{V.1})$$

where α is a constant and L_A is the length of the boundary of region A . The area term, represented by αL_A , satisfies the conditions of the Venn diagram:

$$\mathcal{I}_L(A : B) = L_A + L_B - L_{A \cup B} - L_{A \cap B} = 0. \quad (\text{V.2})$$

Thus, the SSA condition for S_{TEE} holds if and only if the SSA for S_{EE} is satisfied. Since the SSA condition for S_{EE} is guaranteed by the properties of the von Neumann entropy, it follows that we can expect the SSA for S_{TEE} to also hold.

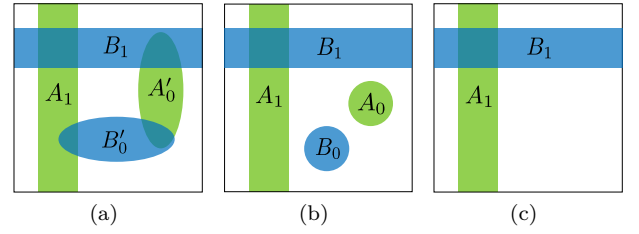


FIG. 6. The schematic diagram for the three steps: (a) which is the general case where A'_0, B'_0 represent the contractible subregions and A_1, B_1 represent the non-contractible ones, (b) where all contractible regions are deformed such that they are isolated, and (c) where A, B become ribbons after the contractible isolated regions are removed.

In this sections, we will demonstrate, through topological properties, that the SSA for S_{TEE} holds if and only if Eq. (I.6) is satisfied. This provides an alternative perspective on the SSA that does not depend on any specific detailed model. Our discussion proceeds in three steps.

First, we isolate any contractible region $A'_0 \subset A'$ by deforming A'_0 to A_0 such that A_0 is isolated from other parts. We will show that conditional mutual information increases when intersections occur. Therefore, the SSA condition for general cases can be reduced to those where all contractible regions are isolated.

Next, we use the surgery method to demonstrate that the SSA condition is invariant under the removal of contractible, isolated regions. This further simplifies the problem, leaving us with cases where regions A and B consist solely of torus knot ribbons.

Finally, we classify these cases by the intersection number i_{AB} between the torus knots of A and B . We show that the SSA condition for both the TEE and the iTEE holds for $i_{AB} \geq 2$ and $i_{AB} = 0$. Moreover, we show

that the SSA for $i_{AB} = 1$ holds if and only if Eq. (I.6) is satisfied.

Although we are unable to prove the general validity of Eq. (I.6), we have verified its correctness for unitary modular categories up to rank 11 [27], including the Fibonacci anyon and the semion model. Thus, we conjecture that it holds for all unitary modular categories. Conversely, we have found that Eq. (I.6) is violated in non-pseudo-unitary modular categories, such as the Yang-Lee anyon. This suggests that modifications to either Eq. (V.1) or the TEE calculation may be necessary.

A. Isolating contractible regions

Let $A' = A_1 \amalg A'_0$, where A_0 is a contractible region with $A_0 \cap B \neq \emptyset$. We can always homotopically deform A'_0 to a new region A_0 such that $A_0 \cap B = \emptyset$. [35] In this subsection, we aim to show that \mathcal{I}_{TEE} will only decrease when a contractible region becomes isolated (i.e., when intersections are removed). This can be equivalently shown by demonstrating that \mathcal{I}_{TEE} will only increase when intersections occur. To be more precise, we consider the difference in \mathcal{I}_{TEE} between the deformed and original configurations:

$$\Delta \mathcal{I}_{\text{TEE}} = \mathcal{I}_{\text{TEE}}(A', B) - \mathcal{I}_{\text{TEE}}(A, B) \geq 0, \quad (\text{V.3})$$

where $A = A_1 \amalg A_0$ is the configuration with A_0 being isolated. For convenience, we will refer to $A = A_1 \amalg A_0$ as the original region and $A' = A_1 \amalg A'_0$ as the deformed region. Throughout this subsection, all changes denoted by Δ represent the gain after the intersections occur.

Intuitively, $\mathcal{I}_{\text{TEE}}(A, B)$ measures the conditional mutual information between regions A and B . Any increase in intersections between the two subregions should increase the shared information, leading one to expect that $\mathcal{I}_{\text{TEE}}(A, B)$ will increase as intersections occur [36].

By induction, it suffices to consider the case where A_0 is a connected component of A [37] as the argument can then be extended to cases with multiple components. We will prove by contradiction, assuming that $\Delta \mathcal{I}_{\text{TEE}}(A, B) < 0$, meaning

$$\Delta(S_{\text{TEE}}(A) + S_{\text{TEE}}(B) - S_{\text{TEE}}(A \cup B) - S_{\text{TEE}}(A \cap B)) < 0. \quad (\text{V.4})$$

Since the $A \simeq A'$, we have $\Delta(S_{\text{TEE}}(A) + S_{\text{TEE}}(B)) = 0$, and thus

$$\Delta(S_{\text{TEE}}(A \cup B) + S_{\text{TEE}}(A \cap B)) > 0. \quad (\text{V.5})$$

Given that $S_{\text{TEE}} = S_{i\text{TEE}} + S_{\text{gs}}$, this leads to two possibilities: either

$$\Delta \mathcal{I}_{i\text{TEE}} = -\Delta(S_{i\text{TEE}}(A \cup B) + S_{i\text{TEE}}(A \cap B)) < 0, \quad (\text{V.6})$$

or

$$\Delta \mathcal{I}_{\text{gs}} = -\Delta(S_{\text{gs}}(A \cup B) + S_{\text{gs}}(A \cap B)) < 0. \quad (\text{V.7})$$

We will first show in Sec V A 1 that $\Delta \mathcal{I}_{i\text{TEE}} \leq 0$ and then demonstrate in Sec. V A 2 that $\Delta \mathcal{I}_{\text{gs}} > 0$ implies $\Delta \mathcal{I}_{\text{TEE}} \leq 0$. In either case, we reach a contradiction to our assumption, thus proving the claim.

$$1. \quad \Delta \mathcal{I}_{i\text{TEE}} \geq 0$$

In this subsection, we aim to show $\Delta \mathcal{I}_{i\text{TEE}} \geq 0$. Using Eq. (IV.13), it suffices to show

$$2\Delta \mathcal{I}_{\pi} - 2\Delta \mathcal{I}_{\text{g}} - \Delta \mathcal{I}_{\chi} \leq 0. \quad (\text{V.8})$$

We observe that $\Delta \mathcal{I}_{\chi}$ vanishes, since

$$\Delta(\chi_{A \cup B} + \chi_{A \cap B}) = \Delta(\chi_A + \chi_B) = 0. \quad (\text{V.9})$$

Therefore, it remains to show that $\Delta \mathcal{I}_{\pi} \leq \Delta \mathcal{I}_{\text{g}}$, or equivalently,

$$\Delta(\pi_{A \cup B} + \pi_{A \cap B}) \geq \Delta(g_{A \cup B} + g_{A \cap B}). \quad (\text{V.10})$$

We first consider the left-hand side of Eq. (V.10). Let us decompose $A_1 \cup B = \amalg_i C_i$ into connected components. After the deformation, let A'_0 intersect with B at the first n C_i components, i.e., $A_0 \cap C_i \neq \emptyset, \forall i \leq n$. Each intersection $A'_0 \cap C_i$ contains at least one component, i.e., $\pi_{A'_0 \cap C_i} \geq 1$. The region $A' \cup B$ gains $\Delta \pi_{A \cap B} = \sum_{i=1}^n \pi_{A'_0 \cap C_i} \geq n$ new intersections. On the other hand, the n components of $A_1 \cup B$ connect with A_0 , reducing the number of components, so $\Delta \pi_{A \cup B} = -n$. Thus, we have

$$\Delta(\pi_{A \cup B} + \pi_{A \cap B}) = \sum_i \pi_{A'_0 \cap C_i} - n \geq 0. \quad (\text{V.11})$$

For the right-hand side of Eq. (V.10), note that $g_{A'_0 \cap B} = 0$, since A'_0 is contractible and so is $A'_0 \cap B$. Therefore,

$$\Delta g_{A \cap B} = \Delta g_{A_1 \cap B} + \Delta g_{A_0 \cap B} = g_{A'_0 \cap B} = 0, \quad (\text{V.12})$$

where $\Delta g_{A_1 \cap B} = 0$ since A_1 is not deformed. If $\Delta g_{A \cup B} = 0$, then by Eq. (V.11), the proof is complete. Now, suppose $\Delta g_{A \cup B} = 1$. Since the genus can either be 0 or 1, this implies $g_{A \cup B} = 0$ and $g_{A' \cup B} = \sum_{i=1}^n g_{A'_0 \cup C_i} = 1$. Without losing generality, let $g_{A'_0 \cup C_1} = 1$. Since $C_1 \subset A \cup B$, by Eq. (IV.5), we have $g_{C_1} \leq g_{A \cup B} = 0$. Therefore, $g_{C_1} = 0$, meaning that C_1 contains no torus cycle. Thus, every cycle in $A'_0 \cup C_1$ must intersect A'_0 at an interval (see Fig. 7 for example). Therefore, A'_0 must intersect with B twice, at two disjoint components at the entrance and exit (see Appendix A for a more detailed derivation). Consequently, we have $\pi_{A'_0 \cap C_1} \geq 2$, which gives $\sum_{i=1}^n \pi_{A'_0 \cap C_i} \geq n + 1$. Thus, we can conclude:

$$\begin{aligned} & \Delta(\pi_{A \cup B} + \pi_{A \cap B}) - \Delta(g_{A \cup B} + g_{A \cap B}) \\ &= \sum_{i=1}^n \pi_{A'_0 \cap C_i} - n - 1 \geq 0. \end{aligned} \quad (\text{V.13})$$

This completes the proof of Eq. (V.6).

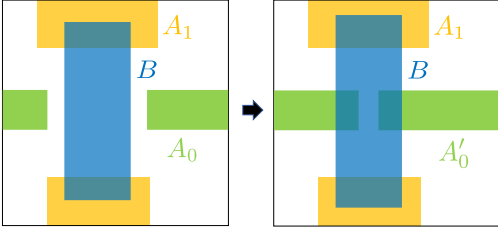


FIG. 7. An example where $\Delta g_{A \cup B} = 1$ and $\Delta \pi_{A \cap B} = 2$.

2. $\Delta \mathcal{I}_{\text{gs}} < 0$ implies $\Delta \mathcal{I}_{\text{TEE}} \geq 0$

In this subsection, we will show that $\Delta \mathcal{I}_{\text{gs}} < 0$ implies $\Delta \mathcal{I}_{\text{TEE}} = -\Delta(S_{\text{iTEE}}(A \cup B) + S_{\text{iTEE}}(A \cap B)) \geq 0$. Since

$$\Delta S_{\text{TEE}}(A \cap B) = S_{\text{TEE}}(A'_0 \cap B) \leq 0, \quad (\text{V.14})$$

it suffice to show that $\Delta \mathcal{I}_{\text{gs}} < 0$ will implies $\Delta S_{\text{TEE}}(A \cup B) \leq 0$. Moreover, since A'_0 is contractible, $A'_0 \cap B$ is also contractible. Thus, $A_1 \cap B$ and $A' \cap B = (A_1 \cap B) \amalg (A'_0 \cap B)$ must correspond to the same canonical bipartition. Therefore, we have $S_{\text{gs}}(A \cap B) = S_{\text{gs}}(A_1 \cap B) = S_{\text{gs}}(A' \cap B)$, which implies

$$\Delta S_{\text{gs}}(A \cap B) = 0. \quad (\text{V.15})$$

It follows that we need to demonstrate that $\Delta S_{\text{gs}}(A \cup B) > 0$ implies $\Delta S_{\text{TEE}}(A \cup B) \leq 0$. For $\Delta S_{\text{gs}}(A \cup B) > 0$, $A \cup B$ must gain an additional punctured ribbon component after the deformation (See Fig. 8). Without loss of

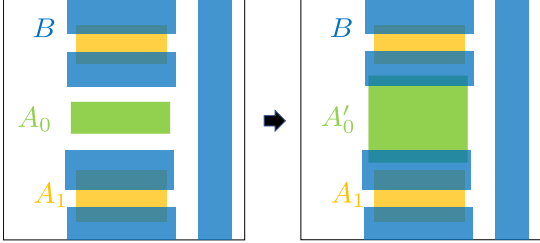


FIG. 8. An example where $A \cup B$ gain an additional punctured ribbon component. In this example, $\Delta S_{\text{gs}}(A \cup B) = \sum_a 2|\psi_a|^2 \ln d_a$, $\Delta S_{\text{iTEE}}(A \cup B) = -2 \ln \mathcal{D}$.

generality, let $A_0 \cup C_1$ be a ribbon component. By assumption, C_1 does not contain the non-contractible loop of $A'_0 \cup C_1$. Therefore, every non-contractible loops of $A_0 \cup C_1$ must go in and out of A_0 , resulting in at least two disjoint intersections, similar to the discussion in Sec. V A 1. Moreover, we find $\Delta g_{A \cup B} = 0$ since $A_0 \cup C_1$ transforms from a punctured disk to a punctured ribbon component. Together with Eq. (V.9), this leads to

$$\Delta S_{\text{iTEE}}(A \cup B) \leq -2 \ln \mathcal{D}. \quad (\text{V.16})$$

On the other hand, from Eq. (III.49), we obtain

$$\Delta S_{\text{gs}}(A \cup B) = \begin{cases} \sum_a 2|\psi_a|^2 (\ln d_a - \ln |\psi_a|), & \text{if } m_{A \cup B} = 0 \\ \sum_a 2|\psi_a|^2 \ln d_a, & \text{if } m_{A \cup B} > 0 \end{cases}, \quad (\text{V.17})$$

where $m_{A \cup B}$ is the number of ribbon components that the original region $A \cup B$ contains. In either case, we find $\Delta S_{\text{gs}}(A \cup B) \leq 2 \ln \mathcal{D}$, leading to $\Delta S_{\text{TEE}}(A \cup B) \leq 0$. This finishes the proof that $\Delta \mathcal{I}_{\text{gs}} < 0$ implies $\Delta \mathcal{I}_{\text{TEE}} \geq 0$.

In summary, we proved by contradiction that if \mathcal{I}_{TEE} decreases upon introducing intersections, then either $\mathcal{I}_{\text{iTEE}}$ or \mathcal{I}_{gs} must decrease. However, both scenarios are impossible because any topological change in a component that aims to decrease the TEE will ultimately necessitate multiple intersections, thereby increasing the TEE even further.

B. Removing contractible isolated regions

From the previous subsection, we established that the SSA for a general bipartition can be inferred from the cases where all contractible components are isolated. In this subsection, we will further demonstrate that the SSA condition remains invariant under the removal of these isolated contractible components.

Since A_0 is a connected component, $A_0 \cap A_1 = \emptyset$, we can apply Eq. (II.7) and obtain:

$$S_{\text{TEE}}(A) = S_{\text{TEE}}(A_0) + S_{\text{TEE}}(A_1). \quad (\text{V.18})$$

Moreover, A_0 is contractible and isolated, $A_0 \cap B = \emptyset$, we obtain:

$$S_{\text{TEE}}(A \cup B) = S_{\text{TEE}}(A_0) + S_{\text{TEE}}(A_1 \cup B). \quad (\text{V.19})$$

Additionally, because $A \cap B = A_0 \cap B \amalg A_1 \cap B = A_1 \cap B$, it follows that:

$$S_{\text{TEE}}(A \cap B) = S_{\text{TEE}}(A_1 \cap B). \quad (\text{V.20})$$

By combining these results, we arrive at:

$$\mathcal{I}_{\text{TEE}}(A, B) = \mathcal{I}_{\text{TEE}}(A_1, B). \quad (\text{V.21})$$

This demonstrates that the SSA condition for A is equivalent to that for A_1 , meaning that A_0 can be removed from the discussion of SSA.

Since any punctured disk components are contractible and isolated, they can be removed when proving the SSA property. Additionally, the complement of a punctured torus component is a punctured disk. Together with Eq. (I.14), which shows that the SSA condition is invariant under the simultaneous complement of A and B , this allows us to remove these components as well when verifying the SSA condition. Furthermore, punctures in connected components act as contractible components under complement operations, meaning they can also be removed. Therefore, what remains is to establish the SSA for cases where both A and B consist solely of ribbon components.

C. The SSA for S_{TEE} for ribbons

From Sec. V A and Sec. V B, we have seen that showing the SSA for S_{TEE} of arbitrary A and B reduces to

showing the SSA for cases where A and B consist solely of ribbon components.

Let A consist of π_A copies of $K(p_A, q_A)$ ribbons and B consist of π_B copies of $K(p_B, q_B)$ ribbons. The minimal number of intersections between them is given by $\pi_A \pi_B i_{AB}$, where $i_{AB} = |q_A p_B - q_B p_A|$ represents the intersection number between $K(p_A, q_A)$ and $K(p_B, q_B)$. In the following, we classify the cases based on i_{AB} .

1. $i_{AB} \geq 2$

For $i_{AB} \geq 2$, the ribbons of A and B do not share the same type of torus knots. Since $A \cap B \subset A, B$, any torus knot of $A \cap B$ must also be contained in both A and B . However, given that A and B do not share the same type of torus knots, this means $A \cap B$ contains no torus knots.

Furthermore, $A \cap B$ has no punctures because neither A nor B have punctures. Hence, all components of $A \cap B$ are disks. For each disk, we have $\chi_{D^2} = \pi_{D^2} = \pi_{\partial D^2} = 1$, so we conclude:

$$\pi_{A \cap B} = \chi_{A \cap B} = \pi_{\partial(A \cap B)}. \quad (\text{V.22})$$

On the other hand, $A \cup B$ must form a punctured torus since it includes two distinct types of non-contractible loops from the torus knots of A and B . For a punctured torus, the number of boundary components equals the number of punctures. Applying Eq. (IV.4) with $g_{A \cup B} = 1$ gives:

$$\pi_{\partial(A \cup B)} = -\chi_{A \cup B} = \chi_{A \cap B}. \quad (\text{V.23})$$

Combining Eq. (V.22) and Eq. (V.23), we obtain the relation:

$$\pi_{\partial(A \cup B)} + \pi_{\partial(A \cap B)} = 2\pi_{A \cap B} \quad (\text{V.24})$$

Since both A and B are annuli, they satisfy $\chi_A = \chi_B = 0$, and each annulus has two boundary components, meaning $\pi_{\partial A} = 2\pi_A$ and $\pi_{\partial B} = 2\pi_B$. Using Eq. (III.52), we obtain the expression:

$$\mathcal{I}_{\text{iTEE}} = -2(\pi_A + \pi_B - \pi_{A \cap B}) \ln \mathcal{D}. \quad (\text{V.25})$$

Since $\pi_{A \cap B}$, the number of intersections between A and B , is bounded by $\pi_A \pi_B i_{AB}$, we have:

$$\pi_{A \cap B} \geq \pi_A \pi_B i_{AB}. \quad (\text{V.26})$$

For the case $i_{AB} \geq 2$, it also holds that $\pi_A \pi_B i_{AB} \geq \pi_A + \pi_B$, which implies:

$$\pi_{A \cap B} \geq \pi_A + \pi_B. \quad (\text{V.27})$$

Thus, we conclude that $\mathcal{I}_{\text{iTEE}} \geq 0$, meaning that the SSA condition for the iTEE holds.

Furthermore, since $S_{\text{gs}}(A \cap B) = S_{\text{gs}}(A \cup B) = 0$, we have $\mathcal{I}_{\text{TEE}} \geq \mathcal{I}_{\text{iTEE}} \geq 0$, which confirms that the SSA holds for both the iTEE and the total TEE S_{iTEE} and S_{TEE} .

2. $i_{AB} = 0$

Next, we consider the case where $i_{AB} = 0$, i.e., the torus knots of A and B are of the same type. Let $A \cup B = \prod_{i=1}^{\pi_{A \cup B}} C_i$ be the decomposition into connected components. Since each C_i must contain at least one connected component of A or B , it must contain the torus knot of A or B . Therefore, it is either a punctured ribbon or a punctured torus.

Suppose C_1 is a punctured torus, i.e., $g_{C_1} = 1$, then it must contain a torus knot K whose intersection number with A and B is one. Since different types of torus knots must intersect, all components of A and B must be connected through K . That is, $A \cup B$ is connected, i.e., $\pi_{A \cup B} = 1$. Therefore,

$$\chi_{A \cup B} = 2\pi_{A \cup B} - 2g_{A \cup B} - \pi_{\partial(A \cup B)} = -\pi_{\partial(A \cup B)}. \quad (\text{V.28})$$

On the other hand, since $A \cap B \subset A$ and $g_A = 1$, $g_{A \cap B} = 1$. Therefore,

$$\chi_{A \cap B} = 2\pi_{A \cap B} - \pi_{\partial(A \cap B)}. \quad (\text{V.29})$$

Since A, B are ribbons, $\chi_A = \chi_B = 0$. Thus, $\mathcal{I}_{\chi}(A : B) = 0$ implies

$$\chi_{A \cap B} + \chi_{A \cup B} = 0. \quad (\text{V.30})$$

Adding Eq. (V.28) and Eq. (V.29) to zero yields

$$\pi_{\partial(A \cup B)} + \pi_{\partial(A \cap B)} = 2\pi_{A \cap B}. \quad (\text{V.31})$$

If we follow the process in Sec. IV to construct the graph whose vertices are the connected components of A, B . We will now obtain

$$\text{Edges} \geq \text{Vertices}, \quad (\text{V.32})$$

instead of Eq. (IV.7) since we have a loop K threading through the graph, making the graph not a tree graph.[38] This then implies

$$\pi_{A \cap B} \geq \pi_A + \pi_B. \quad (\text{V.33})$$

Hence,

$$\pi_{\partial(A \cup B)} + \pi_{\partial(A \cap B)} = 2\pi_{A \cap B} \geq 2(\pi_A + \pi_B) = \pi_{\partial A} + \pi_{\partial B}, \quad (\text{V.34})$$

i.e., $\mathcal{I}_{\text{iTEE}}(A : B) \geq 0$. Moreover, since any boundary components of $A \cap B$ is part of A or B , the maximum number of non-contractible boundary that $A \cap B$ can have is $2(\pi_A + \pi_B)$. Therefore, from Eq. (III.48) we have

$$S_{\text{gs}}(A) + S_{\text{gs}}(B) \geq S_{\text{gs}}(A \cup B) + S_{\text{gs}}(A \cap B). \quad (\text{V.35})$$

Combining the results, we have the SSA holds if $A \cup B$ contain a punctured torus component.

Next, suppose non of the C_i is a punctured torus. For such case, we have $\mathcal{I}_g = 0$ and therefore the SSA for S_{iTEE} holds. As for the S_{gs} , let m_X be the number of punctured torus components for X . We have $m_A + m_B \geq$

$m_{A \cup B} + m_{A \cap B}$ since each torus ribbon component of $A \cap B$ will reduce the number of ribbon components of $A \cup B$. Therefore, applying Eq. (III.49) for $m_A, m_B \geq 1$, we have

$$S_{\text{gs}}(A) + S_{\text{gs}}(B) \geq S_{\text{gs}}(A \cup B) + S_{\text{gs}}(A \cap B). \quad (\text{V.36})$$

Combining with the SSA for S_{iTEE} , we then obtain the SSA for S_{TEE} .

As a remark, similar to the case of $i_{AB} \geq 2$, $\mathcal{I}_{\text{iTEE}} \geq 0$ and $\mathcal{I}_{\text{gs}} \geq 0$ hold separately. Furthermore, in Sec. VA1, we have shown that the $\mathcal{I}_{\text{iTEE}}$ will only increase as the intersections occur. Therefore, we have actually shown that the SSA for $\mathcal{I}_{\text{iTEE}}$ holds in general for $i_{AB} \neq 1$ cases.

3. $i_{AB} = 1$

For $i_{AB} = 1$, suppose either $\pi_A > 1$ or $\pi_B > 1$, then Eq. (V.27) is satisfied. Repeating the steps in Sec. VC1, we confirm that both the iTEE and the total TEE, S_{iTEE} and S_{TEE} , respectively, satisfy the SSA condition.

For the remaining cases, without loss of generality, we can assume $(\pi_A, \pi_B) = (1, r)$, where $r \in \mathbb{Z}_{>0}$ is a positive integer. From Sec. VC1, we know that $A \cap B$ consists entirely of disks, while $A \cup B$ forms a punctured torus. For both $A \cup B$ and $A \cap B$, the ground state entropy S_{gs} vanishes. Furthermore, using Eq. (V.24) and Eq. (V.26) we get:

$$S_{\text{iTEE}}(A \cap B) + S_{\text{iTEE}}(A \cup B) \leq -2r \ln \mathcal{D}, \quad (\text{V.37})$$

which implies

$$S_{\text{TEE}}(A \cap B) + S_{\text{TEE}}(A \cup B) \leq -2r \ln \mathcal{D}, \quad (\text{V.38})$$

Additionally, we have:

$$S_{\text{iTEE}}(A) + S_{\text{iTEE}}(B) = -2(r+1) \ln \mathcal{D}. \quad (\text{V.39})$$

Thus, it remains to determine S_{gs} for A and B combined. Since $|q_{APB} - q_{BPA}| = 1$, we can apply the Euclidean algorithm to transform A, B into a meridian ribbon and longitude ribbons, respectively. This indicates that the states for A and B are related by a modular S transformation. Applying Eq. (III.48), the general ground state entropy for A and B combined is:

$$\begin{aligned} & S_{\text{gs}}(A) + S_{\text{gs}}(B) \\ &= \sum_a 2|\psi_a|^2 (\ln d_a - \ln |\psi_a|) + 2|S\psi_a|^2 (r \ln d_a - \ln |S\psi_a|). \end{aligned} \quad (\text{V.40})$$

Since the second term increases as r increases, it suffices to check the case where $r = 1$. Therefore, the SSA for $i_{AB} = 1$ holds if and only if the following inequality is satisfied:

$$\sum_a |\psi_a|^2 (\ln d_a - \ln |\psi_a|) + |S\psi_a|^2 (\ln d_a - \ln |S\psi_a|) \geq 2 \ln \mathcal{D}. \quad (\text{V.41})$$

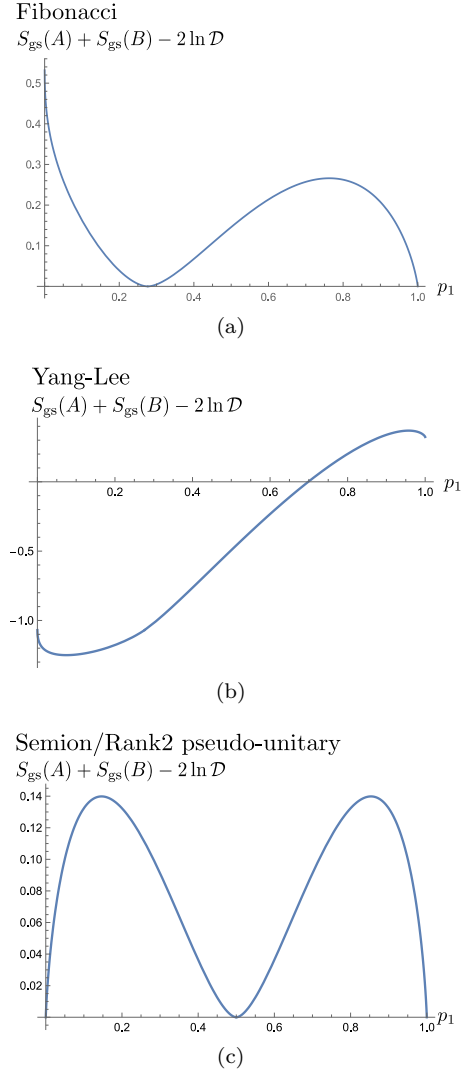


FIG. 9. $S_{\text{gs}}(A) + S_{\text{gs}}(B) - 2 \ln \mathcal{D}$ as a function of $p_1 = |\psi_1|^2$ for (a) Fibonacci anyon, (b) Yang-Lee anyon, (c) Semion/pseudo-unitary partner (their figures are identical). Eq. (I.6) holds if the graph is above zero.

Although we are unable to prove this inequality, we can verify the condition for existing modular data classified by [39]. For example, at rank 2, we examine the Fibonacci anyon and its non-pseudo-unitary counterpart, the Yang-Lee anyon. Their modular S matrices are given by:

$$S^{\text{Fib}} = \begin{pmatrix} 1 & \frac{1-\sqrt{5}}{2} \\ \frac{1+\sqrt{5}}{2} & -1 \end{pmatrix}, \quad S^{\text{YL}} = \begin{pmatrix} 1 & \frac{1-\sqrt{5}}{2} \\ \frac{1+\sqrt{5}}{2} & -1 \end{pmatrix}. \quad (\text{V.42})$$

As shown in Fig. 9, the Fibonacci anyon satisfies Eq. (V.41) while the Yang-Lee anyon does not. We also consider the semion anyon and a pseudo-unitary anyon in its Galois

orbit, with their respective modular S matrices:

$$S^{\text{Sem}} = \begin{pmatrix} 1 & 1 \\ 1 & -1 \end{pmatrix}, \quad S^{\text{PU}} = \begin{pmatrix} 1 & -1 \\ -1 & -1 \end{pmatrix}. \quad (\text{V.43})$$

Interestingly, the TEE behavior for the semion and its pseudo-unitary partner is identical.

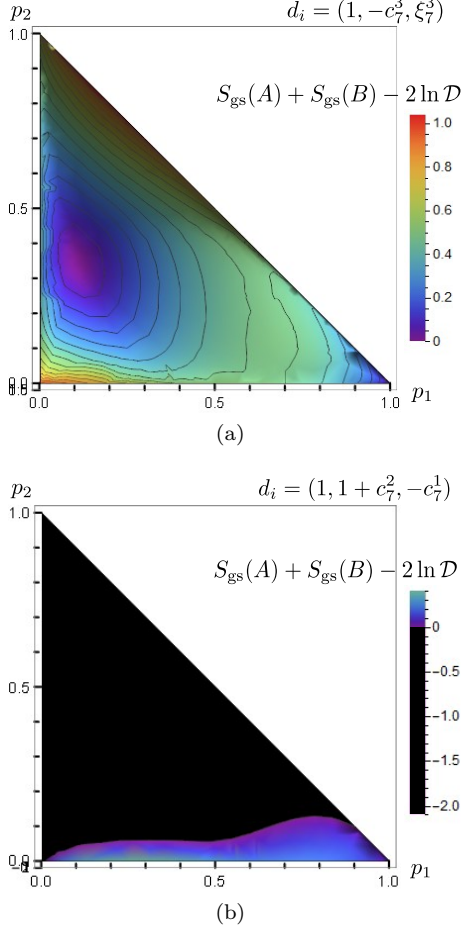


FIG. 10. $S_{\text{gs}}(A) + S_{\text{gs}}(B) - 2 \ln \mathcal{D}$ as a function of p_1, p_2, p_3 subject to $p_1 + p_2 + p_3 = 1$ for (a) a unitary rank 3 anyon and (b) one of its non-pseudo-unitary partner. The black region indicates the parameter spaces where Eq. (I.6) is violated.

As an example of a unitary modular category at rank 3, we consider one with the modular S matrix:

$$S = \begin{pmatrix} 1 & -c_7^3 & \xi_7^3 \\ -c_7^3 & -\xi_7^3 & 1 \\ \xi_7^3 & 1 & c_7^3 \end{pmatrix}, \quad (\text{V.44})$$

where $c_m^n = \zeta_m^n + \zeta_m^{-n}$, $\xi_m^n = \frac{\zeta_{2m}^n - \zeta_{2m}^{-n}}{\zeta_{2m}^1 - \zeta_{2m}^{-1}}$, and $\zeta_m^n = e^{\frac{2n\pi i}{m}}$ are the cyclotomic numbers.

A non-unitary (and also non-pseudo-unitary) Galois partner of this model has the modular S matrix:

$$S = \begin{pmatrix} 1 & 1 + c_7^2 & -c_7^1 \\ 1 + c_7^2 & c_7^1 & 1 \\ -c_7^1 & 1 & -1 - c_7^1 \end{pmatrix}, \quad (\text{V.45})$$

from Fig. 10, we observe that the unitary model satisfies Eq. (V.41), while its non-unitary Galois partner does not.

We have verified that Eq. (V.41) holds for all unitary modular categories classified in Ref. [39] up to rank 11 [27]. Based on these findings, we conjecture that this condition is universally true for any unitary modular category.

D. Violation of SSA for S_{iTEE}

In the proof of SSA for S_{TEE} , we demonstrated that removing contractible subregions further strengthens the SSA for both S_{iTEE} and S_{TEE} . Moreover, we established that the SSA for S_{iTEE} holds in cases where $i_{AB} = 0$ or $i_{AB} \geq 2$. Thus, the only possible violation of the SSA for S_{TEE} occurs when $i_{AB} = 1$. Specifically, this violation happens when $(\pi_A, \pi_B) = (1, r)$ for some $r \in \mathbb{N}_+$, as illustrated Fig. (VD) (up to a coordinate transformation). In such cases, we have $\mathcal{I}_{\text{iTEE}} = -2 \ln \mathcal{D}$. Any additional

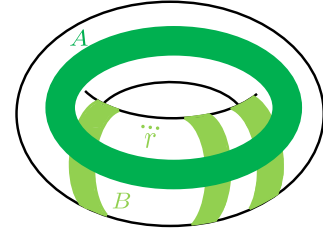


FIG. 11. The only cases where $\mathcal{I}_{\text{iTEE}} \leq 0$.

removable intersections would contribute at least $2 \ln \mathcal{D}$ to $\mathcal{I}_{\text{iTEE}}$, causing the SSA to hold.

VI. Conclusion

In this paper, we classify different bipartitions of a torus based on their entanglement interfaces. Each bipartition consists of an even number of torus knots of the same type, along with other contractible loops. By removing bubbles and applying coordinate transformations, any bipartition can be reduced to a canonical form, which features an even number of meridians.

Using the replica and generalized surgery methods, we compute the topological entanglement entropy (TEE) for canonical bipartitions and arbitrary bipartitions. We find that the TEE decomposes into three components: S_{iTEE} , which depends on the number of interfaces; S_{Wil} , a weighted sum of the contributions from Wilson lines; and S_{cl} , a classical contribution due to superpositions between different ground states. The Wilson line and classical contributions appear only when a non-contractible interface is present.

Building on these results, we derive a modified strong subadditivity condition for the intrinsic TEE, given by $\mathcal{I}_{\text{iTEE}}(A : B) \geq 2\mathcal{I}_{\text{g}}(A : B) \ln \mathcal{D}$, using purely topological

arguments. Here, $\mathcal{I}_g(A : B)$ is a term that depends on the genus of the subregions and is bounded by $|\mathcal{I}_{gs}(A : B)| \leq 1$. This modified condition deviates from the usual SSA only when $\mathcal{I}_{gs}(A : B) = -1$. The configurations that satisfy $\mathcal{I}_{gs}(A : B) = -1$ correspond to the cases where regions A and B take the form shown in Fig. VD. For all other configurations, the intrinsic TEE satisfies the standard SSA condition $\mathcal{I}_{TEE}(A : B) \geq 0$.

We also discuss about the SSA for the total TEE. By removing the isolated and contractible regions, we are able to reduce our discussion to the cases where A, B are torus knot ribbons. We classify the cases by the intersection number i_{AB} between the torus knots. For $i_{AB} \neq 1$, we have proven that the SSA indeed holds. When $i_{AB} = 1$, we demonstrate that the SSA holds if and only if Eq. (V.41) is satisfied. Numerical verification confirms that Eq. (V.41) is indeed true for unitary modular categories up to rank 11 [27], leading us to conjecture that this condition may hold for all UMTCs. This suggests that Eq. (V.41) might impose implicit constraints on possible UMTCs.

However, we also observe that Eq. (V.41) can be violated for non-unitary MTCs, such as the Yang-Lee anyon. This indicates that the SSA for S_{TEE} might be violated for such non-unitary MTCs. Nevertheless, applying Eq. V.1 together with the SSA for the entanglement entropy S_{EE} one can still derive the SSA for S_{TEE} . Therefore, this raises the possibility that either Eq. (V.1) or the current method for calculating TEE might require modification for non-unitary MTCs.

VII. Acknowledgments

We are grateful to Xueda Wen for useful discussions. P.-Y.C. acknowledges support from the National Science and Technology Council of Taiwan under Grants No. NSTC 113-2112-M-007-019. Both P.-Y.C and C.-Y. L. thank the National Center for Theoretical Sciences, Physics Division for its support.

A. Some related proof 1

In Sec. VA, we have given a heuristic argument that suppose $A \cup B$ contains a cycle which is not contained in either A or B , then A and B must intersect at least twice. In this appendix, we give a more rigorous proof to the statement.

Let C be a cycle of $A \cup B$ that is not contained in either A or B , and C_{A_0} be a connected component of $C \cap A$. Suppose every connected component of $C \cap A$ are contained in B , then $C = (C \cap A) \cup (C \cap B) = B$ which is a contradiction. Therefore, Without loss of generality we assume that $C_{A_0} \not\subset B$. Since $C \simeq S^1$, we can let $C = [0, 2]$ with end points identified. Since C is not contained in B , $C_{A_0} \neq C$. Therefore, $C_{A_0} \simeq (0, 1)$ is a proper open subset of C . We can then assume $C_{A_0} =$

$(0, 1)$ Without loss of generality. Let B_0 and B_1 be the connected component that contain 0 and 1. Since B open and $i \in B_i$, thus there exists an open interval in B_i that intersects with C_{A_0} . Furthermore, if C_{A_0} and C_{A_1} were to be in the same connected component of $A \cap B$, then we must have either $(1, 2) \subset A \cap B$ or $(0, 1) \subset A \cap B$. If $(1, 2) \subset A \cap B$, then $A = C$ which is a contradiction. On the other hand, if $(0, 1) \subset A \cap B$, then $C_{A_0} \subset B$ which is also a contradiction. Therefore, $A \cap B$ must contain at least two connected components which contains C_{A_0} and C_{A_1} respectively.

B. Some related proof 2

Let $A = \Pi_{i=1}^{\pi_A} A_i$, $B = \Pi_{j=1}^{\pi_B} B_j$ be the decomposition into connected components. Consider the new torus cycle C of $A \cup B$ and let $a_i = A_i \cap C$, $b_j = B_j \cap C$. We create a graph whose vertices are a_i and b_j . We draw $|\partial a_i \cap b_j|$ directional edges from a_i to b_j , where $0 \leq |\partial a_i \cap b_j| \leq 2$ is the number of boundary points of a_i in b_j . Similarly, we draw $|\partial b_j \cap a_i|$ directional edges from b_j to a_i . For each vertices, there are exactly two edges pointing outward, i.e., Edges = $2(\pi_A + \pi_B)$. Furthermore, Since a_i 's are disjoint, there are no edges between them. Moreover, there are no isolated vertices since $A \cup B$ is connected. Next, we claim that there are exactly zero or two edges connecting each vertices. Without loss of generality, suppose that there is a boundary point of a_i in b_j . Either $a_i \subset b_j$ or $\partial b_j \cap a_i \neq \emptyset$. Therefore, either the other boundary point of a_i is also in b_j or exactly one boundary point of b_j is in a_i . Either case, there are exactly two edges between them. For each $a_i \cap b_j$ contributing to the connected component of $A \cap B$ there are exactly two edges between a_i and b_j . Therefore,

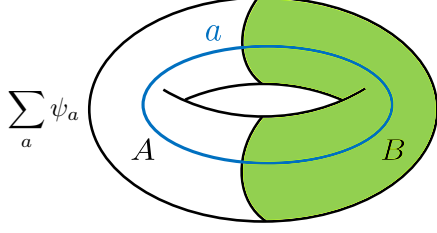
$$\pi_{A \cap B} \geq \frac{1}{2} \text{Edges} = \pi_A + \pi_B. \quad (\text{B.1})$$

Note that the equality might not holds since there might be other intersections of A_i and B_j beside the component intersecting with C .

C. Edge approach

Here, we will briefly review the edge approach used in Ref. [21] to compute the TEE. The key idea is that entanglement between the two subregions can be reduced to the entanglement between the left and right moving sectors of the edge state at the interface [23]. First, one consider the R_1 bipartition where there is a single inter-

face encircling the Wilson line



The regularized edge state can be described by

$$|\psi\rangle = \sum_a \psi_a |\mathfrak{h}_\alpha\rangle, \quad (\text{C.1})$$

where

$$|\mathfrak{h}_\alpha\rangle = \frac{e^{-\epsilon H}}{\sqrt{\mathfrak{n}_\alpha}} |h_\alpha\rangle \quad (\text{C.2})$$

normalizes the Ishibashi state

$$|h_\alpha\rangle = \sum_{N=0}^{\infty} \sum_{j=1}^{d_{h_\alpha}(N)} |h_\alpha, N; j\rangle \otimes \overline{|h_\alpha, N; j\rangle}. \quad (\text{C.3})$$

The reduced density matrix is then obtained by tracing out the anti-chiral sector

$$\rho_L = \sum_{a, N, j} |\psi_a|^2 \frac{e^{\frac{8\pi\epsilon}{l}(h_a + N - \frac{c}{24})}}{\mathfrak{n}_a} |h_a, N; j\rangle \langle h_a, N; j|. \quad (\text{C.4})$$

After some calculation and taking the thermodynamic limit $\frac{l}{\epsilon} \rightarrow \infty$, one arrive at

$$\text{Tr} \rho_L^n \rightarrow \sum_a e^{\frac{\pi c l}{48\epsilon}} |\psi_a|^{2n} (S_{0a})^{1-n}. \quad (\text{C.5})$$

Multiplying by $\frac{1}{1-n}$ and taking the $n \rightarrow 1$ limit, one then obtain the entanglement entropy as

$$S_{\text{EE}} = \frac{\pi c l}{24\epsilon} - \ln \mathcal{D} + \sum_a |\psi_a|^2 \ln d_a - \sum_a |\psi_a|^2 \ln |\psi_a|^2, \quad (\text{C.6})$$

which is exactly the $m = 1$ case for Eq. (III.48) with an extra area contribution $\frac{\pi c l}{24\epsilon}$.

Such approach can also be generalized to the R_m bipartition we have been considering by simply tensoring the edge states.

$$|\psi\rangle = \sum_a \psi_a |\otimes_{k=1}^m \mathfrak{h}_\alpha\rangle_k, \quad (\text{C.7})$$

where the k is the ring label. Repeating similar process, one can obtain that

$$\text{Tr} \rho_L^n \rightarrow \sum_a e^{\frac{\pi c l}{48\epsilon}} |\psi_a|^{2n} (S_{0a})^{2m(1-n)}, \quad (\text{C.8})$$

which yields

$$S_{\text{EE}} = \frac{\pi c l}{24\epsilon} - m \ln \mathcal{D} + m \sum_a |\psi_a|^2 \ln d_a - \sum_a |\psi_a|^2 \ln |\psi_a|^2. \quad (\text{C.9})$$

This is exactly Eq. (III.48) with an extra area contribution.

-
- [1] X. G. WEN, *International Journal of Modern Physics B* **04**, 239 (1990), <https://doi.org/10.1142/S021797929000139>.
- [2] L. D. Landau, in *Collected Papers of L.D. Landau*, edited by D. ter Haar (Pergamon, 1965) pp. 193–216.
- [3] D. C. Tsui, H. L. Stormer, and A. C. Gossard, *Phys. Rev. Lett.* **48**, 1559 (1982).
- [4] R. B. Laughlin, *Phys. Rev. Lett.* **50**, 1395 (1983).
- [5] X.-G. Wen, *Phys. Rev. B* **65**, 165113 (2002).
- [6] M. Stone and S.-B. Chung, *Phys. Rev. B* **73**, 014505 (2006).
- [7] E. Witten, *Communications in Mathematical Physics* **121**, 351 (1989).
- [8] M. F. Atiyah, *Publications Mathematiques de IHES* **68**, 175 (1988).
- [9] J. Maldacena, *International Journal of Theoretical Physics* **38**, 1113 (1999).
- [10] L. Susskind, *Journal of Mathematical Physics* **36**, 6377 (1995), https://pubs.aip.org/aip/jmp/article-pdf/36/11/6377/19188778/6377_1_online.pdf.
- [11] A. Kitaev and J. Preskill, *Phys. Rev. Lett.* **96**, 110404 (2006).
- [12] M. Levin and X.-G. Wen, *Phys. Rev. Lett.* **96**, 110405 (2006).
- [13] M. Haque, O. Zozulya, and K. Schoutens, *Phys. Rev. Lett.* **98**, 060401 (2007).
- [14] O. S. Zozulya, M. Haque, K. Schoutens, and E. H. Rezayi, *Phys. Rev. B* **76**, 125310 (2007).
- [15] B. A. Friedman and G. C. Levine, *Phys. Rev. B* **78**, 035320 (2008).
- [16] S. V. Isakov, M. B. Hastings, and R. G. Melko, *Nature Physics* **7**, 772 (2011).
- [17] H.-C. Jiang, Z. Wang, and L. Balents, *Nature Physics* **8**, 902 (2012).
- [18] C. Castelnovo and C. Chamon, *Phys. Rev. B* **76**, 184442 (2007).
- [19] S. Furukawa and G. Misguich, *Phys. Rev. B* **75**, 214407 (2007).
- [20] S. Dong, E. Fradkin, R. G. Leigh, and S. Nowling, *Journal of High Energy Physics* **2008**, 016 (2008).
- [21] X. Wen, S. Matsuura, and S. Ryu, *Phys. Rev. B* **93**, 245140 (2016).
- [22] J. Cardy, in *Encyclopedia of Mathematical Physics*, edited by J.-P. Francoise, G. L. Naber, and T. S. Tsun (Academic Press, Oxford, 2006) pp. 333–340.
- [23] X.-L. Qi, H. Katsura, and A. W. W. Ludwig, *Phys. Rev.*

- Lett. **108**, 196402 (2012).
- [24] D. Das and S. Datta, *Phys. Rev. Lett.* **115**, 131602 (2015).
- [25] S. Ryu and T. Takayanagi, *Phys. Rev. Lett.* **96**, 181602 (2006).
- [26] T. Takayanagi, *Classical and Quantum Gravity* **29**, 153001 (2012).
- [27] The numerical data is available <https://github.com/chihyulo/SSA-of-TEE-for-UMTC-up-to-rank-11>.
- [28] X. Wen, P.-Y. Chang, and S. Ryu, *Journal of High Energy Physics* **2016**, 12 (2016).
- [29] For simplicity, we will discuss the case without Wilson line insertions. However, the argument remains valid in the presence of Wilson lines.
- [30] Any Wilson lines should be avoided in this consideration.
- [31] C.-Y. Lo and P.-Y. Chang, *Journal of High Energy Physics* **2024**, 117 (2024).
- [32] A simple way to compute the number of holes F is to apply the Euler characteristic formula with $\chi = 1$, $E = 4n$ and $V = 4$.
- [33] The gray line is actually continuous; the diagram is simplified for ease of visualization.
- [34] P. Bonderson, K. Shtengel, and J. Slingerland, *Annals of Physics* **323**, 2709 (2008).
- [35] We exclude the trivial case where $B^c = \emptyset$, as the SSA condition is trivial in that scenario. If $B^c \neq \emptyset$, there exist an open set $U \subset B^c$. Therefore, we can homotopically move and contract A'_0 to A_0 such that $A_0 \subset U \subset B^c$.
- [36] This intuition is not universally true. For example, consider the case where A and B are disjoint R_1 bipartitions, for which $\mathcal{I}_{\text{TEE}}(A : B) = S_{\text{cl}}$. If we introduce an intersection between A and B at a ring region, we obtain $\mathcal{I}_{\text{TEE}}(A : B) = 0$, meaning that the conditional topological mutual information actually decreases when the intersection is introduced.
- [37] We consider the case where there are finite connected components.
- [38] For an alternative but relatively rigorous proof, see Appendix B.
- [39] S.-H. Ng, E. C. Rowell, and X.-G. Wen, *Classification of modular data up to rank 11* (2023), [arXiv:2308.09670 \[math.QA\]](https://arxiv.org/abs/2308.09670).